May 2014

Spectral Analysis of Flame Emission for Optimization of Combustion Devices on Marine Vessels

Panagiota Stamatoglou

Supervisor: Mattias Richter

Division of Combustion Physics
Department of Physics
Lund University

Master of Science Thesis

Spectral Analysis of Flame Emission for Optimization Of Combustion Devices on Marine Vessels

LUNDS UNIVERSITET

Panagiota Stamatoglou
Master of Science Thesis

Supervisor: Mattias Richter

Division of Combustion Physics
Department of Physics
Lund University
Kockumation Group, Malmö(Sweden)

May 2014

Lund, Sweden, May 2014

Lund Reports on Combustion Physics LRCP-176
ISNR LUTFD2/TFC-176-SE
ISSN 1102-8718

Panagiota Stamatoglou
Division of Combustion Physics
Department of Physics
Lund University
P.O.Box 118
S-221 00 Lund, Sweden

Στους γονείς μου, Πολυχρόνη και Χρυσή,

με την στήριξη και την αγάπη σας, τα πάντα είναι εφικτά..

Abstract

Chemiluminescent emission from OH^*, CH^* and C_2^* radicals and its dependence on the equivalence ratio is being investigated in the current study. The aim of this project is to use the results for combustion control on marine vessels and safety checks. The study was conducted in collaboration with Kockumation, a leading company in developing control systems for running boilers and steam turbines on marine vessels. Experiments were conducted at laboratory burners as well as an industrial burner, similar to the one that Kockumation uses. A new detection system for flame monitoring was suggested after the evaluation of the current detectors. The use of photodiodes were proven to be more reliable in detecting the chemiluminescent emission across a wide wavelength range (from UV to near IR region). Furthermore, after the analysis of the data, the CH^*/OH^* intensity ratio was evaluated as a calibration model for the prediction of the equivalence ratio. In addition to this, the partial least square regression (PLS-R) based multivariate calibration model was tested and the two models were compared. The latter model showed better accuracy in predicting Φ values. New experiments are also suggested for the investigation of additional species that are involved in the combustion process and the further optimization of combustion devices on marine vessels.

Acknowledgements

Mattias Richter! My super, supportive, kind supervisor with a sense of humour that few people have. Thank you so much for everything! Marcus Aldén and the rest of the people in the division of Combustion Physics, thank you for being a second family to me, I can feel nothing but grateful for the time that I've spent in the Enoch Thulin building. Especially, I would like to thank my lab partner Fahed, you were more helpful that you can imagine my friend. Thank you, Vladimir, for always providing the best solution to my problems! Thank you Yann for your friendship! I would also like to thank the "gang" from room E324...Dina, Sandra, Jianfeng, Samuel, nothing would have been the same without you. Most of all, thank you Dina Hot for being supportive, helpful, inspiring..for being a true friend! During my studies here in Lund, I met a lot of people, some of them I keep closer to my heart: Thank you Chryssa, Fabian, Karolina and Kenneth for your love and support! Last but not least, I would like to thank my family, my friends back home and Alexis for always being there for me. Thank you all!

Contents

Chapter 1

Introduction

1.1 The Importance of Studying Combustion Processes

Combustion processes have always intrigued human curiosity, since the early existence of mankind. According to Greek mythology, fire was provided to humans by Prometheus as a precious gift, an action that caused him a severe punishment by the Olympian gods. The discovery and, most important, the control of fire had an enormous impact on the formation of civilization and its constant development.

Combustion researchers nowadays concentrate on developing new diagnostic techniques and new type of fuels, as an attempt to achieve the highest possible efficiency and the lowest fuel consumption, but also protect the environment from the emissions. In order to achieve that, many experiments are being run, investigating the molecular species that are involved in combustion processes, for gaining an in-depth knowledge of the combustion mechanism. The constant technological development along with the continuously changing needs of the society will determine the future role of combustion on the planet; it will continue to be an important process for energy conversion, also after the transition to renewable fuels.

Molecular spectroscopy is widely used by combustion researchers in various diagnostic techniques, such as Laser Induced Fluorescence (LIF), Laser Induced Incandescence (LII), Coherent anti-Stokes Raman Spectroscopy (CARS) and Chemiluminescence. Especially in the latter, flame emission is being studied as well as its dependence on several combustion parameters, such as equivalence ratio (Φ)[1], temperature and species that are being involved. Each molecule emits electromagnetic radiation at specific wavelengths, which makes that emission unique for a certain molecule. This procedure is the most common used for the identification and characterization of molecules inside a flame.

A molecule, whose emission intensity highly depends on temperature and can be detected in rich flames is carbogen (CH). Furthermore, the molecule with the the highest emission intensity, around stoichiometric conditions, is hydroxide (OH). Another important intermediate species in the combustion reaction is diatomic carbon (C_2), which is usually present in rich flames. The development of molecular physics has lead to an almost complete molecular database, still being upgraded. Modern scientists have more tools and access to knowledge than the previous generations, which has resulted in a rapidly, technologically

[1]
$$\Phi = \frac{(\text{number of moles fuel/number of moles oxidizer})_{real}}{(\text{number of moles fuel/number of moles oxidizer})_{stoich}} \tag{1.1}$$

driven, science revolution.

From a simple household burner to the complete combustion chamber of an engine, combustion has great impact in everyday life. Since the world demands more energy power with the least possible impact on the environment, new energy sources will be used and the use of some of the old ones will be limited or perhaps abandoned.

In this project, spectrally resolved analysis of flame emission is used in order to investigate the various combustion parameters such as equivalence ratio, chemiluminescent intensity, particle emission and their influence to the combustion process. The aim of this project is to study the chemiluminescence of the flame and use the results for combustion control and safety checks. The end application is burner control in steam generators (boilers) for marine propulsion. The work is performed in collaboration with Kockumation, a leading company in this sector. This study could also be of relevance to the boiler system that is used for the central housing heating in Sweden.

1.2 Kockumation

Kockumation Group is a technologically advanced organisation consisting of three worldwide known companies: *Kockum Sonics*, *Texon Automation* and *Polarmarine*.
Kockums Mekaniska Verkstad was founded in 1840 and the main production of the company had been rolling stocks. In 1873 the construction of the first ship was completed and not long after that, the company established itself as one of the leading forces in the design and construction of ships. Additional global recognition was gained with the invention of TYFON by Mr Helge Rydberg and the patent of the product in 1920. Furthermore, Kockums was the first company which delivered the world's first all-welded merchant vessel in 1940 and by the end of 1950 it was one of the biggest ship yards in the world [22].

At present, Kockumation, which has its roots in Kockums, has expanded its activity. Each subcompany is responsible for providing various services in the vessel industry. *Kockum Sonics* has inheritated the technological knowledge and product development of the well -known Kockum Shipyard. Moreover, this company is in charge of the distribution of the product line and software such as TYFON (the acoustic signal system), LOADMASTER (loading computers), LEVELMASTER (level gauging systems), the SHIPMASTER (cargo and ballast automation) and INSONEX (sonic cleaning for marine applications).

Texon Automation, which was part of Kockum Shipyard, was founded in 1976. This company is most focused on control engineering and combustion process engineering. The high quality service that the company offers to the customers includes combustion controls, burner management system (BMS), boil off gas (BOG) control systems as well as flame monitoring.

Polarmarine Skandinavia was founded in 1978 as the daughter company of *Polamarine International*. The company has been involved with development and design of tank cleaning machines; more than 70,000 of them being installed until now. *Polarmarine* offers a wide range of products such as fixed machines, submerged machines and portable machines. Furthermore, the activities of the company cover crude, chemical, product, bulk carriers as well as offshore vessels.

This collaboration has led to new product developments covering loading computers, boiler automation, tank cleaning equipment, cargo and ballast automation, ship's whistles and sonic cleaning systems.

Chapter 2

Theory

2.1 Flame and Combustion

Flame is the result of an exothermic chemical reaction and can be divided into four sub-categories, depending on how the fuel and the oxidizer are being mixed as well as the flame's flow characteristics. A flame is called premixed when the unburned fuel and the oxidizer are mixed prior to reaching the reaction zone whereas in a diffusion flame they mix as they burn. Furthermore there are two different kind of flames, according to the actual flow conditions, laminar and turbulent flames. In a laminar flame the burning velocity of the flame is equal to the fuel flow rate, in contrary to a turbulent flame, where the reactant gas is forced to move towards the flame front at a higher speed than the flame speed due to flame wrinkling [14].

Flame propagates through space in a wave form. There are two types of combustion waves: detonation waves and deflagation waves. The latter, which are the waves that the current study investigates, are the most common in the combustion process. Detonation waves are supersonic waves supported by an exothermic reaction as they travel through a highly combustible medium, such as a methane-air mixture in this case. On the other hand, deflagation waves are subsonic waves propagated by heat release and mass transport from chemical reactions [16].

In order to generate a laminar premixed flame the gas flow is considered to be laminar and uniform across the diameter of the burner. There is a conservation of mass and momentum before and after the flame ignition. The two conservation equations are given bellow [14].
Conservation of mass:

$$\sigma_u S_u = \sigma_b S_b = \dot{m} \tag{2.1}$$

Conservation of momentum:

$$p_u + \sigma_u S_u^2 = p_b + \sigma_b S_b^2 \tag{2.2}$$

where the subscripts u and b refer to unburned and burned gas respectively. S_u is the laminar burning velocity which is the speed that the flame front has while it propagates towards the unburned mixture. The mass flow rate is referred as $m^{\cdot}$, p is the symbol of pressure and σ refers to density.

When the input volumetric gas flow rate (F) and the flame area (A) are known, the burning velocity v_b of the flame can be calculated as follows [9]:

$$v_b = \frac{F}{A}[\frac{cm^3/s}{cm^2}] \tag{2.3}$$

During the combustion process intermediate species, such as radicals, are being produced. These radicals, such as OH, CH and C_2 are not present in the final combustion stage. In the end, only the products that are stable exist. Combustion products can be, for example, a mixture of water vapour, carbon dioxide and nitrogen [18]. The temperature of these products is around 2000 Kelvin and its value depends on the type of the fuel, the equivalence ratio and highly on "buffer" gases such as nitrogen. The temperature at the same equivalence ratio will vary significantly between a fuel/oxygen mixture and a fuel/air mixture. Equivalence ratio (Φ) is the ratio of the real fuel-air ratio to the stoichiometric fuel-air ratio.[1]

The equivalence ratio indicates whether there is an excess of fuel or an excess of oxidizer in the combustion process. In the first case, the mixture is called *rich* ($\Phi > 1$) whereas in the latter, the mixture is called *lean* ($\Phi < 1$). In the stoichiometric condition ($\Phi = 1$) close to complete combustion is achieved by supplying matched amount of fuel and oxidizer to a burner. The laminar flame speed at stoichiometric conditions is the highest possible and a great number of studies, see fig 2.1, have been made in order to calculate the flame speed at different equivalence ratios and for different fuel types.

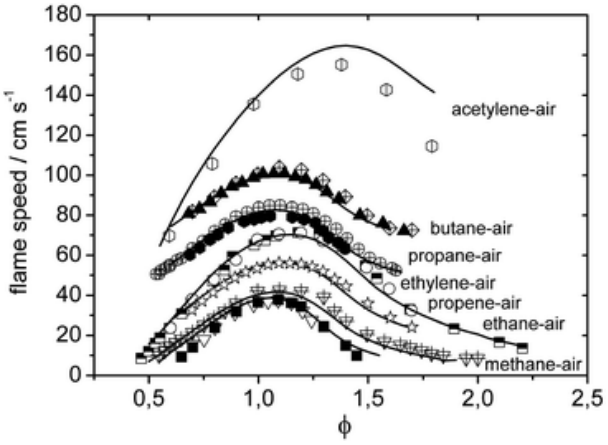

Figure 2.1: Numerically and experimentally determined laminar flame speeds for various C1-C4 (number of carbon atoms) fuels $p = 1bar, T_u = 298K$ (after Ahmed *et al.*) [1]

According to the above figure, the flame speed decreases in rich and lean flames while it reaches the highest value around stoichiometric conditions. Therefore, that should be considered during the preparation of the experiment when the total flow, that is inserted into the burner, has to be determined, see eq 2.3. The input total gas flow depends on the dimension of the burner and the gas composition.

Otherwise, flame stabilization problems such as *flash-back* or *blow-off* may occur during the experiment. If the gas flow is too low, the burning velocity will exceed the gas velocity, which will result in the propagation of the flame downstream, towards or even into the

[1] The stoichiometric fuel-air ratio is calculated using the chemical reaction
$C_xH_y + n_{air}(O_2 + 3.762N_2) \rightarrow xCO_2 + (y/2)H_2O + 3.762n_{air}N_2$[16]
where we consider as air a mixture of nitrogen (79%) and oxygen (21%).

burner tube. That phenomenon is called flash-back and is one of the most common causes of the destruction of Tube/Bunsen burners. There is a critical flow velocity that corresponds to the flash-back limit and is approximately equal to $2S_u/d_T$ [14]. S_u is the laminar burning velocity and d_T is the quenching diameter. Below that diameter, the flame propagation through the pipe of the burner cannot occur. On the other hand, if the gas flow is too high, the flame will rise in order to equalise the flow velocity to the burning velocity, which will eventuallyresult in a extinguishedflame. A flame can also be lifted above the surface of the burner when the mixtureis fuel-rich and the gas velocityis high.

Besides laminar flames there are also turbulent flames, which are more similar to the ones that are used by the industry. The advantage of turbulent flames in contrast to laminar flames is mainly the greater consumption rate of the reactants. Thus there is an increase of the chemical energy release rate and therefore of the power of a certain burner. The factor that determines whether a flame is laminar or turbulent is the *Reynolds number*. The Reynolds number,see eq 2.4 [10] is a dimensionless number that depends on the *kinematic viscosity* (ν_0), the *flow velocity* (U) and the *length* (L) of the tube of the burner.

$$Re = UL/\nu_0 \tag{2.4}$$

where kinematic viscosities of various fuels can be found on-line, in scientific databases, or can be calculated by eq 2.5 [10]; when the representative density ρ_0 and the coefficient of viscosity of a specific fuel are known.

$$\nu_0 \equiv \mu_0/\rho_0 \tag{2.5}$$

According to Hawthorne *et al* [13] a flame with a Reynolds number below 2000 is laminar whereas above that number the flame starts becoming turbulent. The greater the Reynolds number, the higher the turbulence. Results of former studies [17], [13] are presented in fig 2.2. In this figure, the linear dependence of the height of the laminar flame to the flow velocity is shown. The flame height increases until a critical point (breakpoint), after that the flame becomes turbulent and remains in the same height regardless the flow velocity. Another consideration that should be taken into while observing fig 2.2, is that the transition to turbulence starts at the top part of the flame and is gradually moving towards the exit of the jet as the flow velocity increases. When the velocity is high enough the whole flame is turbulent. One notes the transition to turbulence by observing and listening to the flame, since the transition is always accompanied by a loud intense sound and the flame becomes quite unstable and thus more difficult to study.

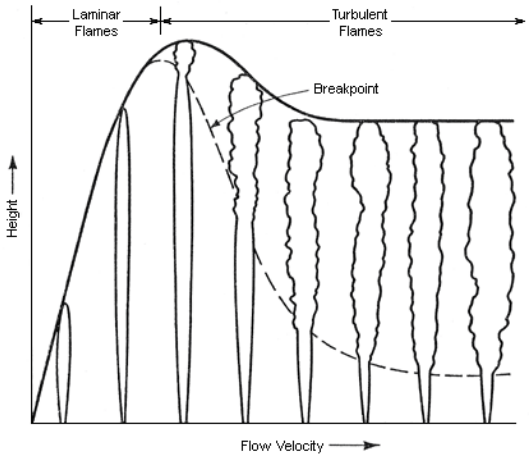

Figure 2.2: Transition from laminar to turbulent flame with increase to gas velocity (after Linan and Williams [17] and Hawthorne *et al* [13]).

In rich flames, another factor that needs to be considered when studying the flame emission is the presence of soot. Soot particles are agglomerates of small, spherical carbonaceous particles that are produced during an incomplete combustion process [16]. Hydrocarbon emission from soot particles is a consequence of the black-body radiation that can be described by three equations [3]:
The Planck distribution law

$$I(\lambda) = \frac{2\pi hc^2}{\lambda^5} \frac{1}{e^{hc/\lambda kT} - 1} \tag{2.6}$$

which gives information about the spectral distribution of the background luminosity. The black-body radiation increases rapidly at longer wavelengths.
The Wien displacement law

$$\lambda_{max} T = 2.898 \cdot 10^{-3} \quad [K \cdot m] \tag{2.7}$$

which determines for each temperature the wavelength with the highest spectral intensity. As the temperature increases, the highest spectral intensity corresponds to shorter wavelengths. The Stefan-Boltzmann law

$$I = \sigma T^4 \tag{2.8}$$

which describes the dependence of the radiation intensity to the flame temperature.

2.2 Molecular Spectroscopy

2.2.1 Chemiluminescence

Chemiluminescence is the emission of electromagnetic radiation by excited molecules, caused by chemical reactions. The excited molecules emit light while they return to a stable condition, i.e. their ground state, a process that is called de-excitation. Each molecule can be identified by studying its emission spectrum and comparing it to other known spectra from previous studies.

In 1900 Max Planck (1858-1947) introduced to the scientific community of that time the quantization of energy of an oscillator. According to Planck [23]:

> "*The oscillator emits in irregular intervals, subject to the laws of chance; it emits, however, only at the moment when its energy of vibration is just equal to an integral multiple n of the elementary quantum* $\epsilon = hv$*, and then it always emits its whole energy of vibration* $n\epsilon$."

where the distinct energy states, in which a molecule can exist, are mentioned for the first time. Any change in energy can only be achieved by a "jump" of the molecule between two energy states. Three of the many kinds of energy that a molecule can have are: *rotational* energy due to the rotation of the molecule about its centre of gravity, *vibrational* energy due to the movement of the atoms around their equilibrium positions, *electronic* energy due to the continuous movement of the electrons [2].

In spectroscopy the emission or absorption spectrum of molecules is what the scientists use in order to characterize each molecule. Consider two electronic energy levels of a molecule for example as shown in fig 2.3:

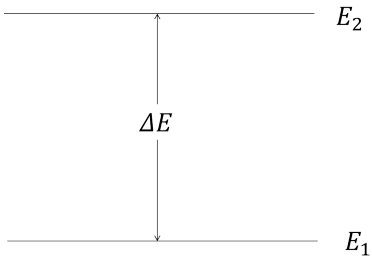

Figure 2.3: Energy difference between two electronic energy states

Transitions can take place between the lowest (E_1) and the highest (E_2) energy levels and vice versa. The energy difference is absorbed or emitted in the form of electromagnetic radiation. A measurement apparatus capable of detecting spectrally resolved radiation is needed, in order to obtain the emission spectrum. The frequency of the emitted radiation is calculated using the following equation [23]:

$$\nu = \Delta E/h \quad [Hz] \tag{2.9}$$

where ν is the frequency of the emitted radiation, ΔE is the energy difference between two energy states and h is Planck's constant. The excited molecules after the emission of radiation return to a lower, stable energy state. Each molecule emits radiation at a different frequency and the chemiluminescent intensity depends on the gas fuel, the flame temperature and the number density of excited molecules thus on the equivalence ratio. Molecules that

are being investigated in the current study are: the *hydroxide* (OH), the *carbogen* (CH) and the *diatomic carbon* (C_2). Measurements are taken in the visible and ultra-violet region thus radiation is emitted mainly due to the electronic transition of molecules.

2.2.2 OH Emission

The excited hydroxide (OH^*) emits radiation in a narrow band at around 308 nm, in the ultraviolet region. OH^* is often used in flame detectors because it emits in the ultra-violet region so the daylight doesn't affect the signal. Thus, no shielding against the visible light is required [27]. Its formation is formed according to the following chemical reaction, suggested by Gaydon(1974) [8]:

$$H + O + M \rightarrow M + OH^* \qquad (R1)$$

where M is any element that can be used as a catalyst in a reaction. The consumption of OH^* is described also by Gaydon [8]:

$$OH^* \rightarrow OH + h\nu \qquad (R2)$$

In the above reactions, OH^* collides with other molecules and exchange energy with them. The highest concentration of OH^* has been observed by Kojima *et al* [15] around stoichiometric conditions. The same study showed a decrease of the intensity of OH^* when taking measurements at richer flames.

2.2.3 CH Emission

The excited carbogen (CH^*) emits radiation in a narrow band at around 431 nm, in the indigo region. CH^* is formed by the following reaction mechanism [14]:

$$C_2 + OH \rightarrow CO + CH^* \qquad (R3)$$

$$O + C_2H \rightarrow CH^* + CO \qquad (R4)$$

$$O_2 + C_2H \rightarrow CH^* + CO_2 \qquad (R5)$$

CH^* is usually used as an indicator of temperature in flame studies. It is a radical that highly depends on the temperature thus it has a strong presence at slightly rich flames ($\phi \simeq 1.1$) [15], where the flame reaches the highest temperature.

2.2.4 C_2 Emission

The excited diatomic carbon (C_2^*) is a radical that is not present at lean flame conditions. It is detected at equivalence ratios $\Phi \geq 1.0$. The reaction mechanism that describes the formation of C_2^* is given bellow [14]:

$$CH_2 + C \rightarrow C_2^* + H_2 \qquad (R6)$$

C_2^* emits in a narrow band at around 513 nm, in the cyan/green region. Another characteristic of this radical is its strong second side band at around 465 nm (blue region). Hardalupas *et al*[12]; Panoutsos *et al*[21] have been studying the chemiluminescence of OH^*, CH^*, C_2^* and its applicability as a heat release indicator. They suggested that OH^* and CH^* are good indicators of the heat release whereas C_2^* is not.

Chapter 3

Experimental Methods

3.1 Experimental Set-up

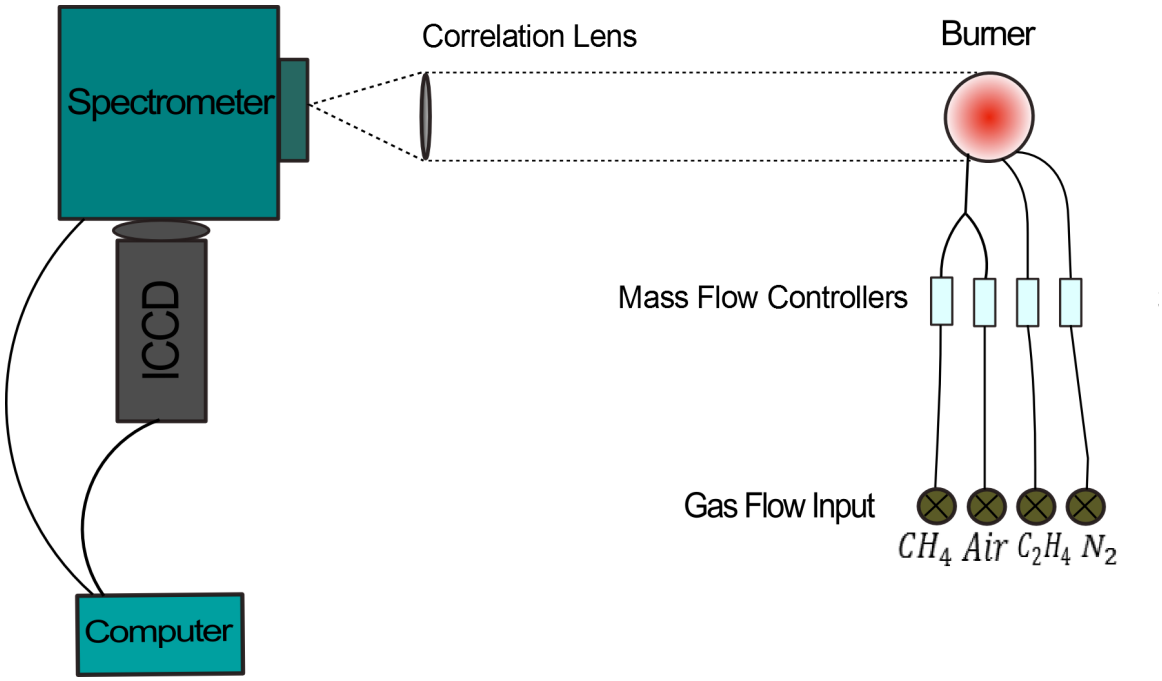

Figure 3.1: Schematic of the experimental set-up.

The same experimental set-up was used three times. The first time a simple McKenna burner was used and the tested fuels were methane and ethylene. The second time, a McKenna with a 1.5 mm nozzle in the middle, running on ethylene, was used. The third time, measurements were taken on an industrial burner, running on Danish natural gas. The industrial burner was similar to the ones that Kockumation uses. Methane (CH_4) is the main component of natural gas, therefore it is commonly used as a substitute for the natural gas. Ethylene (C_2H_4) was used in order to investigate the presence of soot in rich flames.

3.2 Equipment

3.2.1 Spectrometer

A spectrometer is an instrument used in order to split the light that is emitted by a source into different components depending on their wavelength. The spectrometer that was used in this study is an Acton 2300i spectrometer, which consists of a *grating*, that disperses the light into its frequency components, one *spherical mirror* that reflects the inserted light towards a toroidal mirror; the *toroidal mirror* guides the light to the grating, then the dispersed light is guided to another *toroidal mirror* and in the end to an output port where a detector, i.e. ICCD camera (see section 3.2.2), is placed. This kind of spectrometer is used in imaging techniques, since there is spacial resolution along its slit. The grating that was used in the experiments had 300 groves/mm. Gratings have a blazing angle which makes them optimized for different wavelengths, in this case 300 nm. Therefore, the intensities of the individual peaks depends on the spectrometer, the collecting lens and the detector. As a result, the ratios that are being measured are specific to the actual equipment and will vary along different experiments.

3.2.2 ICCD Camera

A PI MAX II ICCD camera, with a 1024 x 1024 (pixels) imaging array, was docked to the spectrometer and was used as a detector. These cameras are used in high resolution imaging and spectroscopy due to their ability to intensify the incoming signal and have very short exposure time.

3.2.3 Flame Sensors

Kockumation uses two different type of flame sensors in order to detect flames. For the ultra violet region, the *R259 UVTRON* flame sensor by *Hamamatsu* is being used whereas for the infra-red region, the *BPX25 silicon planar photo-transistor* by *Ferranti* were considered to be the most suitable. In this study, only the sensitivity curve of the Hamamatsu flame sensors was compared to the obtained spectra since the flame emissions in the UV region were measured. The UVTRON flame sensors have a ON/OFF system that uses the photoelectric effect of metal and the gas multiplication effect of electric current by means of discharge. The sensitivity of the sensors has a narrow range, from 185 nm to 300 nm, making these sensors completely insensitive to visible light. The UVTRON sensors can detect faint ultraviolet emissions from flames, an ability that makes them ideal applicants for fire alarms and arson surveillance.

3.2.4 Laboratory Burners

Two different kind of burners were used in the laboratory: a *McKenna burner* and a *McKenna with a 1.5 mm nozzle burner*. The first one was used in order to study the chemiluminescent emission of a laminar premixed flame; the second one was chosen for the investigation of a sooty turbulent premixed flame. The McKenna burner is often being preferred in flame monitoring experiments because of its applicability to stable, laminar premixed flames due to its large surface area and the existence of a co-flow. The advantage of using the McKenna burner with the nozzle is its ability to produce a turbulent jet flame surrounded by a hot methane-air co-flow, which is burning at stoichiometric conditions.

The presence of the co-flow creates a protecting "shield" that isolates the jet flame from the ambient air. Therefore, the equivalence ratio of the premixed flame at each stage can be accurately estimated.

3.2.5 Industrial Burner

The industrial burner was located at Pågen bakery. The fuel of the burner was Danish natural gas and its composition is presented in table: 3.1. Optical access to the interior of the burner was reached through a circular window after the removal of the glass shielding. Measurements were taken only at the running condition that the company used thus no alterations to the fuel-air ratio were possible.

Table 3.1: Composition of Danish natural gas.

Chemical compound	Chemical formula	Percentage (%)
Methane	CH_4	87.2
Ethane	C_2H_6	6.80
Propane	C_3H_8	3.10
iso-Butane	C_4H_{10}	0.40
n-Butane	C_4H_{10}	0.60
iso-Pentane	C_5H_{12}	0.10
n-Pentane	C_5H_{12}	0.07
Hexane+h	C_{6+}	0.05
Nitrogen	N_2	0.30
Carbon dioxide	CO_2	1.40

3.3 Spectra Acquisition

In the laboratory, before the operation of the burner, a thorough inspection of the gas outlets and the pipe connections was performed in order to detect possible gas leakage. Cooling water was passing through the McKenna burner through out the whole experimental process in order to maintain the temperature of the burner low. The spectra acquisition process was the same to all the experiments. The differences between each experiment were the fuel gas and the type of burner.

Before start taking measurements, the spectrometer should be calibrated by acquiring a spectrum from a light source that has already been studied by others and there are available data for its emission. The light source, that was used in this study for the calibration of the spectrometer, was a mercury lamp. There are many theoretical spectra for the emission of mercury available on the internet. A spectrum was obtained with the spectrometer and three visible peaks (centred at pixel number 218, 510 and 744) were compared to the theoretical ones. These peaks were identified and corresponded to the 365.016 nm, 404.656 nm and 435.833 nm peaks of the theoretical spectrum.

After the identification of the peaks, the actual range of the spectrometer/ICCD combination was estimated to be approximately 139 nm. The wavelength range that needed to be investigated in the current study was larger, therefore two measurements were taken at each equivalence ratio. The spectrometer was centred at 330 nm and 460 nm, respectively.

In addition to the measurements taken at the flame, background emission images were taken in order to reduce the signal-to-noise ratio and offset due to the black-body radiation, by subtracting the background measurement from the flame emission measurement. The measurements were obtained by placing a black, opaque metallic plate in front of the slit of the spectrometer and blocking the flame emission.

Mass flow controllers were used to regulate the gas flow[1] towards the burner. The flame emission was focused on the slit of the spectrometer through a Halle lens (f = 100 mm) and in the end it was guided to the detector, see fig 3.1. The data were stored to a computer and were processed in Matlab. The results of the data processing as well as pictures of the flame by the ICCD camera and a Canon camera are presented at Chapter 4.

[1] Errors in the calculation of the gas flow are estimated in Appendix B.

Chapter 4

Results and Discussion

4.1 McKenna Burner

4.1.1 Premixed Methane-Air Flame

In the first experiment, a McKenna burner was used in order to detect the chemiluminescence of a premixed methane-air flame. The experimental set-up is similar to the one illustrated in fig 3.1. The gas flows that were used are shown in table 4.1. A flame stabilizer was placed 2 cm above the surface of the burner. The adiabatic temperature of a stoichiometric methane-air flame is around 2,200 K but the use of the flame stabilizer can cause a cooling effect on the flame. In addition to the flame stabilizer, a cold co-flow of Nitrogen was used in order to protect the flame from the ambient air and control the local equivalence ratio. The flow of the Nitrogen that was used was 10 l/min, same as the total fuel and air gas flow, in order to keep the same flow velocity and minimize the turbulence as much as possible.

The settings of the ICCD camera were different at each experiment depending on the intensity of the signal. In this experiment, the gain was originally set to 220 but the signal was significantly intense at rich flames, thus the gain was reduced to 180. One should be careful with the applied gain since a high gain can saturatethe camera and damage it. The signal was accumulated10 times by the camera and the exposure time was set to 200 μsec . A short exposure time was used in order not to saturatethe camera.

After each measurement on the flame, an additional measurement of the background luminosity was taken in order to subtract it from the original and thus enhance the signal.

Table 4.1: Gas flows in the premixed methane-air flame at the McKenna burner. The total flow of fuel and air was 10 l/min.

Equivalence ratio (Φ)	F_{CH_4} $[l/min]$	F_{Air} $[l/min]$
0.70	0.68	9.32
0.80	0.77	9.23
0.90	0.86	9.14
1.00	0.95	9.05
1.10	1.04	8.96
1.20	1.12	8.88
1.30	1.20	8.80
1.40	1.28	8.72
1.50	1.36	8.64

Measurements were taken at two different height levels above the surface of the burner. The first set of measurements was taken close to the surface of the burner [∼1.0 cm], where the colour of the flame is bluish. The blue colour of the flame indicates the presence of CH and the more intense the colour is, the largest is the concentration of the excited molecule. The flame, see fig 4.3, has a light blue colour when it is lean and the colour is most intense at $\Phi = 1.1$; an indicator of the strong presence of CH in the flame. In richer flames, green colour is also apparent due to the C_2 emission. A difference between the two set of measurements is that the OH emission in fig 4.2a is higher compared to fig 4.2b. This could be a result of the cooling effect from the flame stabilizer and also the fact that the height in the first case correspond to the primary reaction zone of the flame.

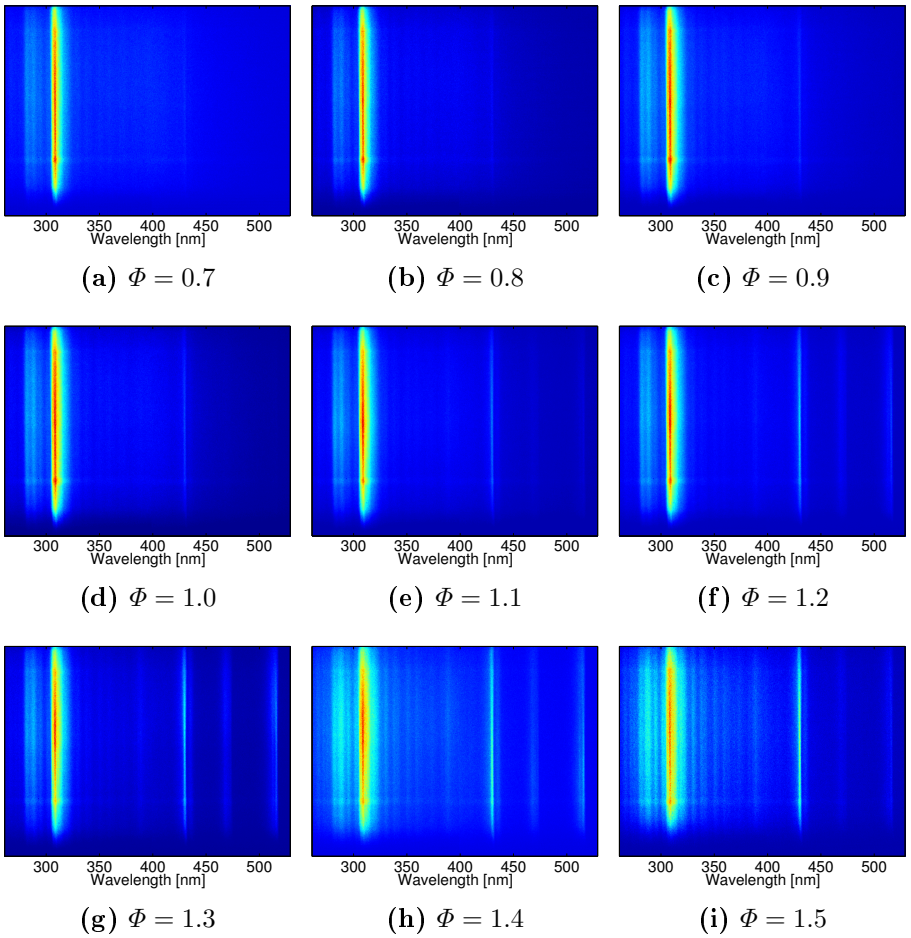

(a) $\Phi = 0.7$ **(b)** $\Phi = 0.8$ **(c)** $\Phi = 0.9$

(d) $\Phi = 1.0$ **(e)** $\Phi = 1.1$ **(f)** $\Phi = 1.2$

(g) $\Phi = 1.3$ **(h)** $\Phi = 1.4$ **(i)** $\Phi = 1.5$

Figure 4.1: Two dimensional emission images obtained by the ICCD camera, at a premixed methane-air flame of a McKenna burner at various Φ. The measurements were taken close to the surface of the burner [∼ 1.0 cm]. The red colour indicates that the signal is strong whereas the light blue colour corresponds to a signal of less intensity. The horizontal axis represents the wavelength region and the perpendicular axis represents the spatial position across the burner.

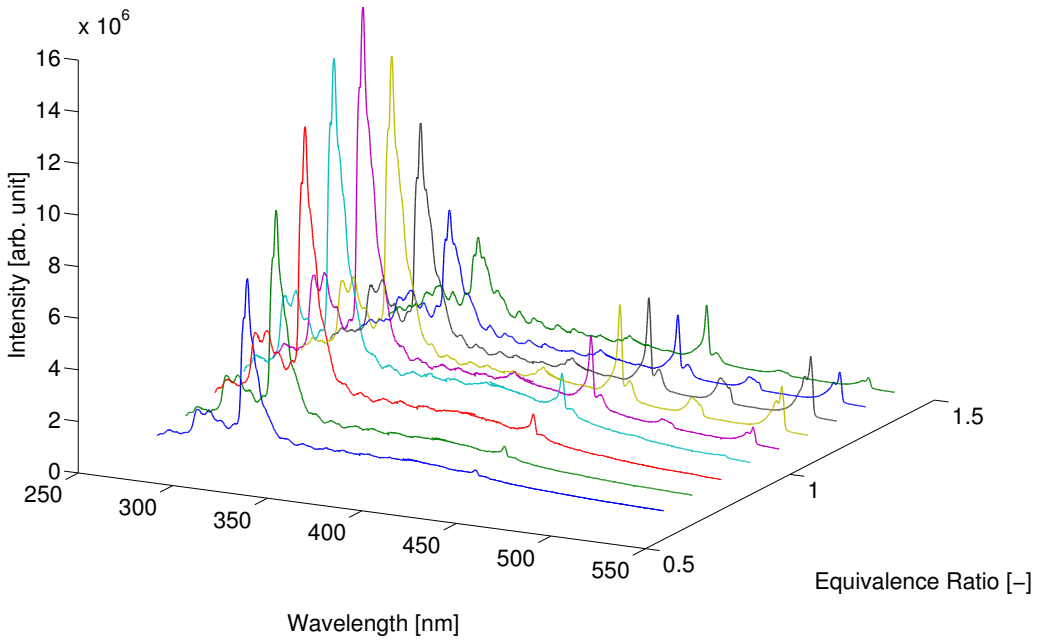

(a) Measurements are taken close to the surface of the burner.

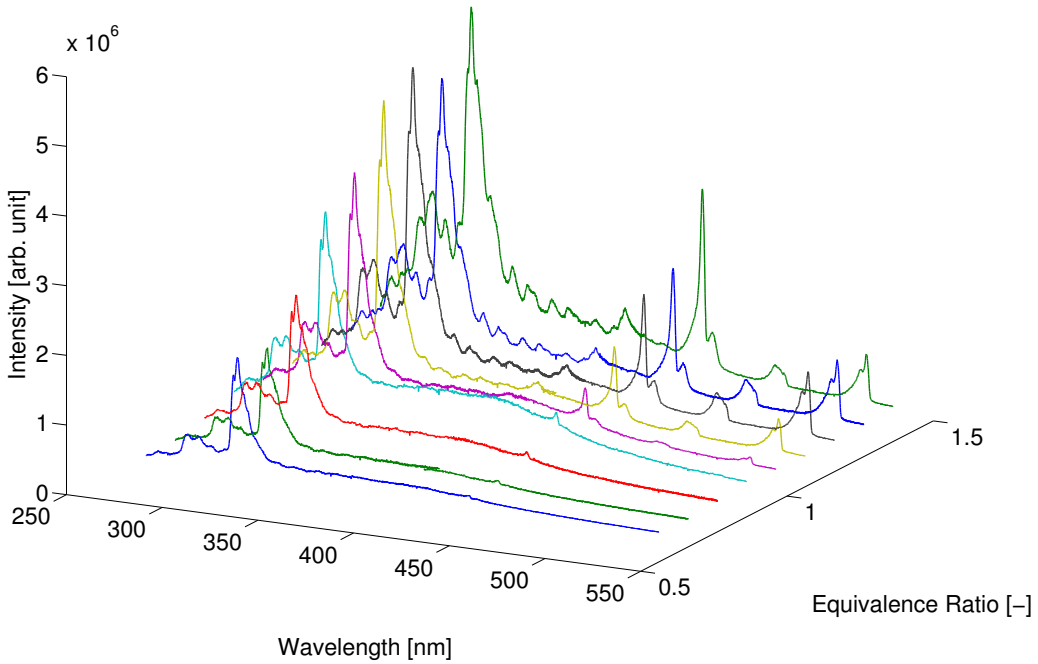

(b) Measurements are taken approximately at 1.5 cm above the surface of the burner.

Figure 4.2: Emission spectra of a premixed methane-air flame at various Φ. The first two peaks, around 280 nm and 308 nm are generated due to the emission of OH. The CH and the two peaks of C_2 can be observed around 429 nm, 467 nm and 515 nm, respectively. Above $\phi = 1.0$ and at $\lambda = 390$ nm, a weaker peak of CH emission can also be observed.

The presence of OH in the flame is stronger around stoichiometric conditions and the highest intensity is observed at $\Phi = 1.1$. The two peaks of OH appeared around $\lambda = 280$ nm and $\lambda = 308$ nm, values that are in accordance with the experimental results of *Hardalupas et al.* [11]. In the same way, the peak of CH is observed at $\lambda = 429$ nm and the two peaks of C_2 at $\lambda = 467$ nm and $\lambda = 515$ nm. The emission of C_2 highly depends on two factors: the temperature and the equivalence ratio. The higher intensity of the emission of C_2 is observed at high temperatures and slightly rich flames. In fig 4.2 its higher intensity corresponds to $\Phi = 1.3$ and it reduces as the flame becomes leaner.

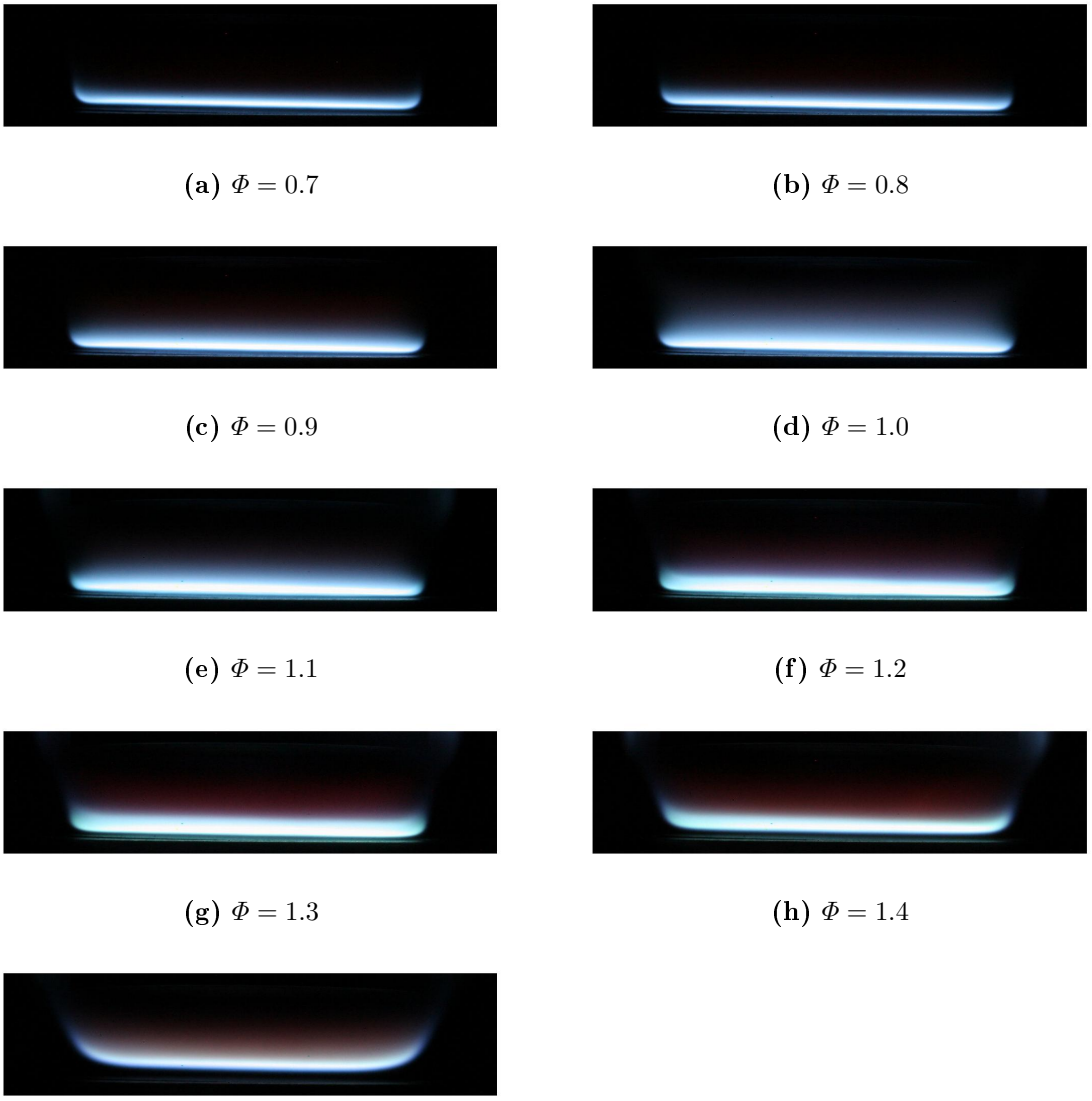

(a) $\Phi = 0.7$ **(b)** $\Phi = 0.8$

(c) $\Phi = 0.9$ **(d)** $\Phi = 1.0$

(e) $\Phi = 1.1$ **(f)** $\Phi = 1.2$

(g) $\Phi = 1.3$ **(h)** $\Phi = 1.4$

(i) $\Phi = 1.5$

Figure 4.3: Pictures of a premixed methane-air flame of a McKenna burner at various Φ values.

4.1.2 Premixed Ethylene-Air Flame

In the second experiment, the same procedure as the previous experiment, see chapter 4.1.1, was followed, using ethylene this time as a fuel. The gas flows that were used are shown in table 4.2. Ethylene, in contrast to methane, is a fuel which produces a significant amount of soot above the stoichiometric equivalence ratio since it contains more carbon atoms. It is an extremely flammable gas, classified as (F^+) according to the *Dangerous Substances Directive* of the European Union [26].

Measurements were taken at two different heights, similar to the first experiment. The first set of measurements was taken close to the surface of the burner [$\sim$ 1.0 cm], see fig 4.5a. The acquired spectra are similar to the spectra in fig 4.2a. In both fig 4.2a and fig 4.5a, the peak of the OH emission has the highest intensity around stoichiometric conditions. In fig 4.2a, the highest intensity of OH is observed at $\Phi = 1.1$ whereas in fig 4.5a, at $\Phi = 1.0$. In addition to the behaviour of OH, the CH and C_2 behave similarly in both cases. In fig 4.5a, the highest intensities of CH and C_2 emissions are noticed at $\Phi = 1.2$ and $\Phi = 1.3$, respectively. In fig 4.5a, the highest peaks of the emission of CH and C_2 are also observed at $\Phi = 1.2$ and $\Phi = 1.3$. The main difference between these spectra is the stronger signal of the ethylene flame, compared to the signal of the methane flame. One reason for this could be that the adiabatic flame temperature of a stoichiometric premixed ethylene flame (air as oxidizer) is 2369 Kelvin [24], higher than in the case of methane.

In the second set of measurements, at approximately 1.5 cm above the surface of the burner, the obtained spectra seem to have been inteferenced by some kind of noise in the signal. Especially at $\Phi = 1.0$, the signal contains a significant amount of noise in both flames, see fig 4.2b and fig 4.5b. On the other hand, it could be the influence of the CO_2 in the spectrum. In the methane flame, fig 4.2b, the higher intensity of OH and CH emission is noticed at $\Phi = 1.5$. This measurement may be influenced by the presence of the flame stabilizer and its cooling effect on the flame. In the ethylene flame, fig 4.5b, the emission of OH is as it was expected, the highest intensity appears at $\Phi = 1.1$ and it remains constant after $\Phi = 1.4$. In rich flames, the colour of the flame above a certain height, see fig: 4.6k-4.6m, is yellowish, which indicates the presence of soot and the dominance of black-body radiation in the spectrum. The chemiluminescent signal is stronger close to the surface of the burner than higher in height. The gain of the ICCD camera was 180 and the exposure time 800 usec, as in the previous experiments with methane.

Table 4.2: Gas flows in the premixed ethylene-air flame at the McKenna burner. The total flow of fuel and air was 10 l/min.

Equivalence ratio (Φ)	$F_{C_2H_4}$ $[l/min]$	F_{Air} $[l/min]$
0.70	0.47	9.53
0.80	0.53	9.47
0.90	0.59	9.41
1.00	0.65	9.35
1.10	0.71	9.29
1.20	0.77	9.23
1.30	0.83	9.17
1.40	0.89	9.11
1.50	0.95	9.05
1.60	1.00	8.99
1.70	1.06	8.94
1.80	1.12	8.88
1.90	1.17	8.83
2.00	1.23	8.77

In fig 4.4n, the yellow colour from the right indicates a strong source of interference due to soot radiation. The signal from the soot is stronger than the one from the chemiluminescent molecules, therefore the signal of C_2 is not apparent beyond $\Phi = 1.9$, see fig 4.5b.

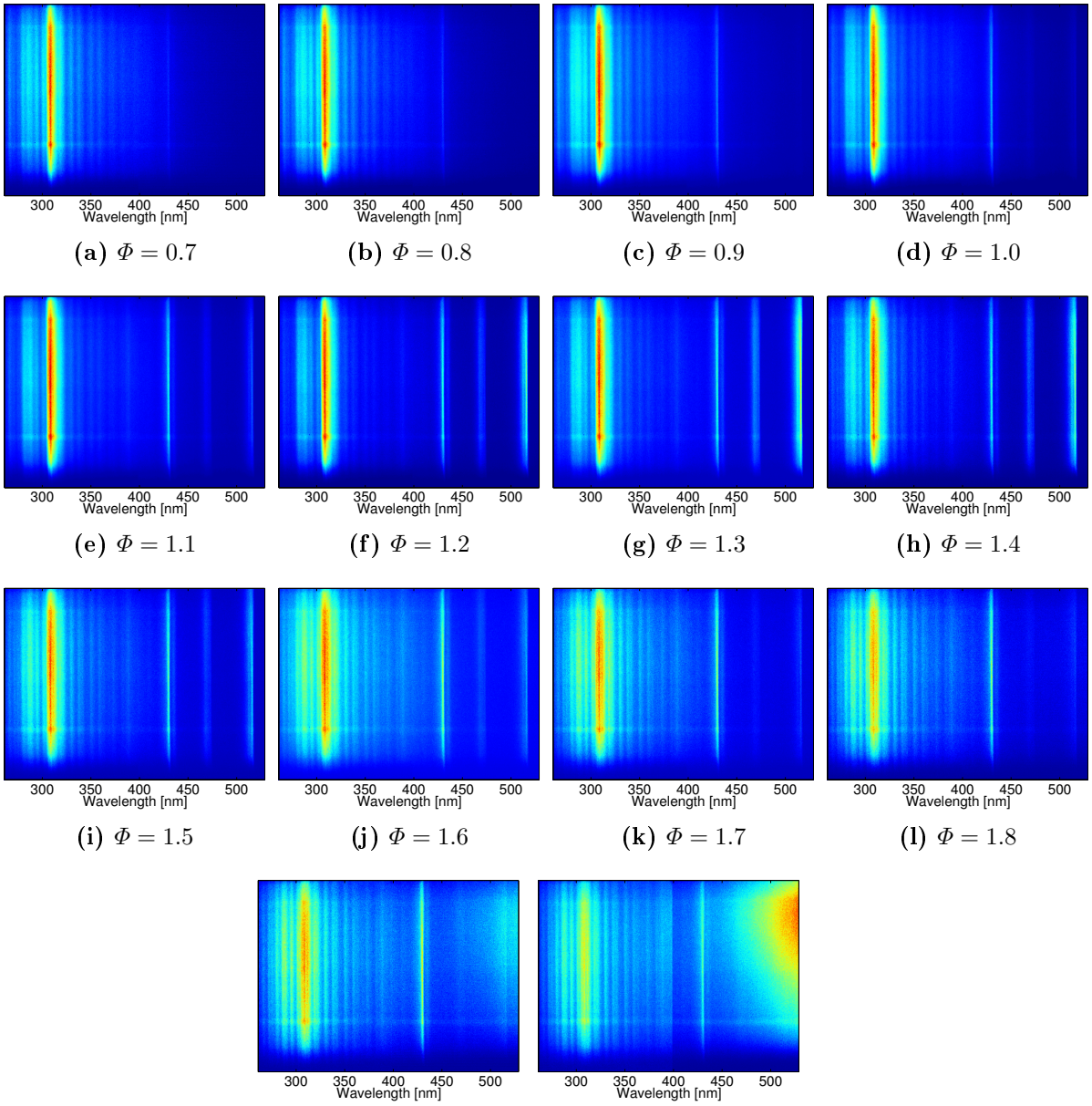

(a) $\Phi = 0.7$ **(b)** $\Phi = 0.8$ **(c)** $\Phi = 0.9$ **(d)** $\Phi = 1.0$

(e) $\Phi = 1.1$ **(f)** $\Phi = 1.2$ **(g)** $\Phi = 1.3$ **(h)** $\Phi = 1.4$

(i) $\Phi = 1.5$ **(j)** $\Phi = 1.6$ **(k)** $\Phi = 1.7$ **(l)** $\Phi = 1.8$

(m) $\Phi = 1.9$ **(n)** $\Phi = 2.0$

Figure 4.4: Two dimensional emission images obtained by the ICCD camera, at a premixed ethylene-air flame of a McKenna burner at various Φ values. The measurements were taken close to the surface of the burner. The red colour indicates that the signal is strong whereas the light blue colour corresponds to a signal of less intensity. The horizontal axes represents the wavelength region and the perpendicular axes represents the spatial position across the burner.

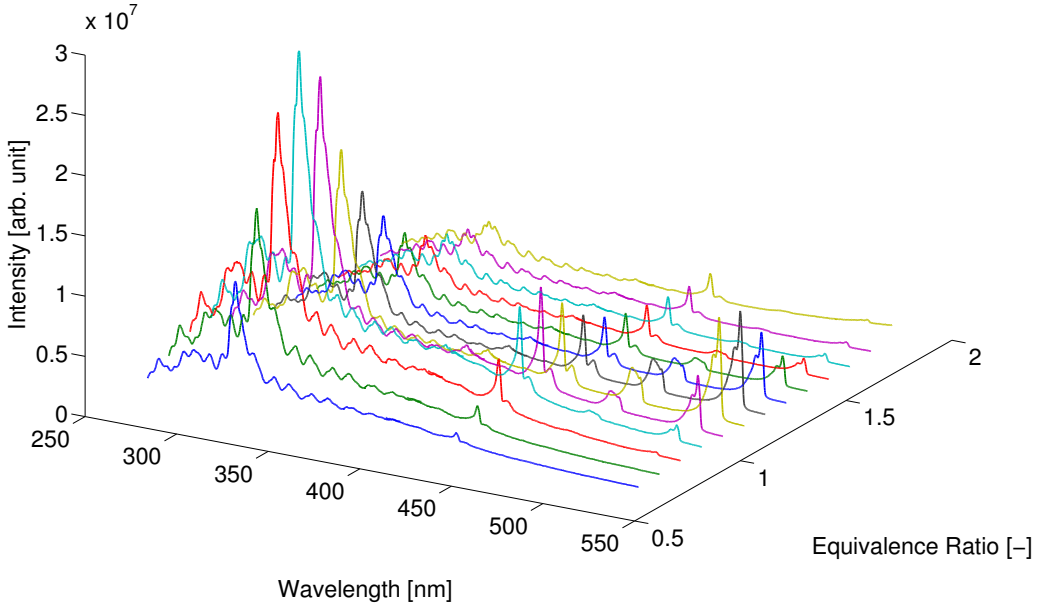

(a) Measurements are taken close to the surface of the burner.

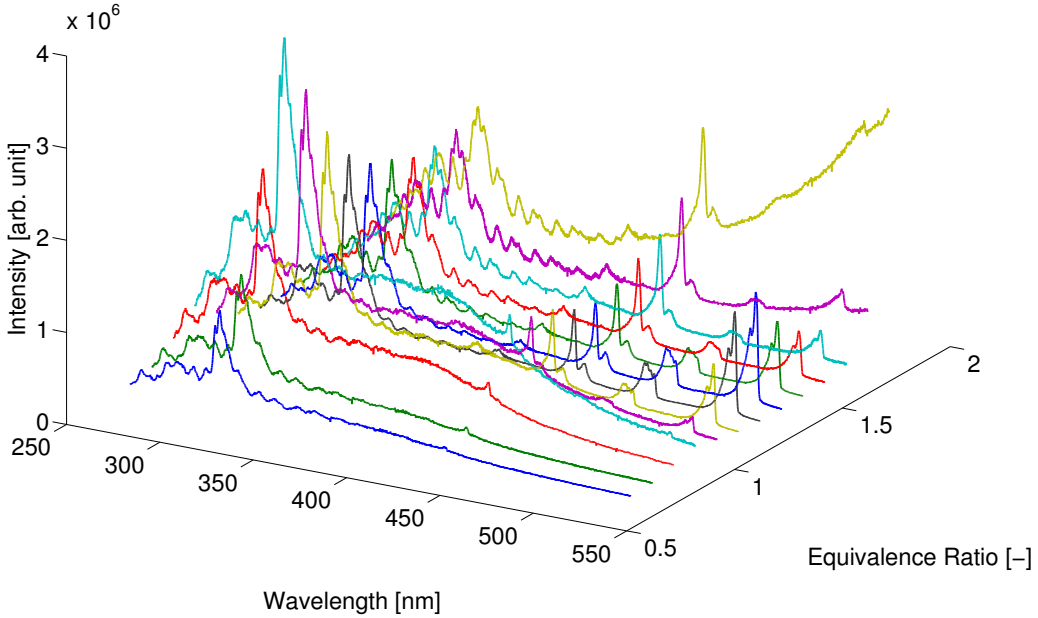

(b) Measurements are taken approximately at 1.5 cm above the surface of the burner.

Figure 4.5: Emission spectra of a premixed ethylene-air flame at various Φ. The first two peaks, around 280 nm and 308 nm are generated due to the emission of OH. The CH and the two peaks of C_2 can be observed around 429 nm, 467 nm and 515 nm, respectively. Above $\phi = 1.0$ and at $\lambda = 390$ nm, a weaker peak of CH emission can also be observed.

(a) $\Phi = 0.7$ **(b)** $\Phi = 0.8$

(c) $\Phi = 0.9$ **(d)** $\Phi = 1.0$

(e) $\Phi = 1.1$ **(f)** $\Phi = 1.2$

(g) $\Phi = 1.3$ **(h)** $\Phi = 1.4$

(i) $\Phi = 1.5$ **(j)** $\Phi = 1.6$

(k) $\Phi = 1.7$ **(l)** $\Phi = 1.8$

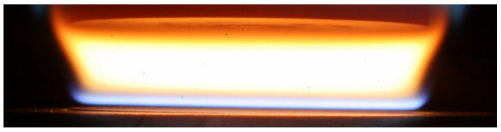

(m) $\Phi = 1.9$

Figure 4.6: Pictures of a premixed ethylene-air flame of a McKenna burner at various Φ values.

4.1.3 Emission Intensity Ratio

A significant amount of studies have used the CH^*/OH^* chemiluminescent intensity ratio of premixed flames as an indicator for the measurement of the equivalence ratio. *M. Orain and Y. Hardalupas* [20] have compared intensity ratios obtained for various fuels such as natural gas, propane, isooctane, ethanol and methanol. The curve of the natural gas [20] is similar to the curve of methane in the current study, since methane is the dominating component in the Danish natural gas.

In fig 4.7, the CH^*/OH^* intensity ratio of the two flames (CH_4/air and C_2H_4/air) was calculated at two different heights. One closer to the surface of the burner (Position 1) and one at around 1.5 cm above the surface (Position 2). Afterwards, the data were plotted versus the measured (from the MFC) equivalence ratio. In fig 4.7a, the 2nd degree curve fitting has been proven to be the most appropriate for the calibration model of the premixed methane flame. The goodness of fit was $R^2 = 0.9957$ and $R^2 = 0.9859$ for position 1 and 2, respectively. The results shown in fig 4.7a can be validated by similar results from previous studies [20],[6],[7],[25],[15]. Any differences in the absolute magnitude of the intensity ratios may occur, due to the different blaze angle (spectrometer grating), wavelength dependant throughout for the collection optics and detector quantum efficiency.

In fig 4.7b, the data of the premixed ethylene flame were fitted to a 3rd degree curve. In position 1, the goodness of fit ($R^2 = 0.9916$) was not as good as the one in the case of methane. On the contrary, in position 2, the goodness of fit was $R^2 = 0.9908$, better than in the methane flame. There are not sufficient data and results from previous studies in order to validate the results of the ethylene flame.

A reason for the difference between the two fuels could be the presence of soot in the ethylene flame. Another difference between the two fuels, that could have influenced the CH^*/OH^* intensity ratio, is the flammability limit. Methane as a fuel is not combustible beyond $\Phi = 1.5$, in contrary to the ethylene, which has a high flammability limit of $\Phi = 2.7$. According to *Tripathi et al.* [25] and *Hardalupas et al.* [12], the CH^*/OH^* intensity ratio model is not suitable for rich equivalence ratios and for the prediction of unknown Φ values. The performance of this calibration model is better at lean flames.

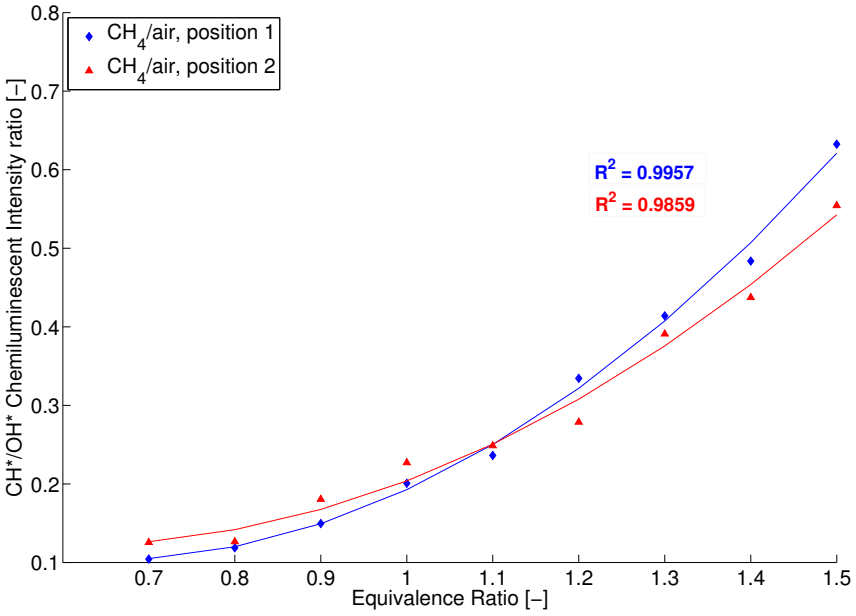

(a) Premixed Methane-air flame

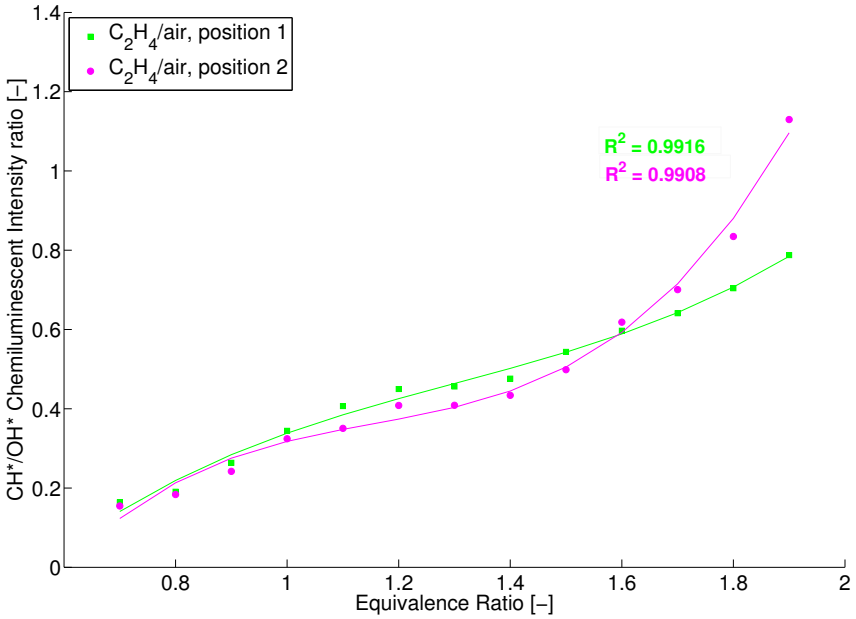

(b) Premixed Ethylene-air flame

Figure 4.7: CH^*/OH^* chemiluminescent intensity ratio as a function of equivalence ratio. Position 1 and 2 correspond to measurements taken close to the surface of the burner and at 1.5 cm above the surface of the burner, respectively. Blue and red curves refer to the premixed methane-air flame, whereas green and pink curves refer to the premixed ethylene-air flame.

4.1.4 PLS-R Based Multivariate Sensing Methodology

A new partial least square regression (PLS-R) based multivariate sensing methodology could also be effective for sensing equivalence ratio in atmospheric methane-air premixed flames, according to a study of *Tripathi et al.* [25]. The advantage of this method compared to the CH^*/OH^* intensity ratio-based calibration model, is the use of the whole spectrum and the conclusion of the contribution of all the involved species. In contrary to the peak intensity ratio, in this method no non-linear background subtraction of CO_2 is required. In the study of *Tripathi et al.* [25], a comparison between both methods was made and the multivariate method showed a better accuracy in predicting the equivalence ratios, especially in rich flames (Φ>1.2).

The PLS-R based multivariate calibration model was used in both premixed methane-air and ethylene-air flames. The data used for the calibration were obtained from the measurements taken close to the surface of the burner. Initially, the number of PLS components used in the calibration model has to be determined. The PLS components show the different directions of variations in the data. The Y-variance indicates how successful the model is in the prediction of unknown data. The larger the percent Y-variance, the better the model is.

The number of PLS components is critical since the higher it is, the more accurate the data will fit to the calibration curve. On the other hand, if too many PLS components are used, the model may try to over-fit the data, which will result in modelling "noise". In fig: 4.8, the residual validation Y-variance is presented as a function of the number of PLS components for the two flames. For the methane flame, see fig: 4.8a, it was decided to use 4 PLS components, whereas for the ethylene flame, see fig: 4.9b, 5 components were used.

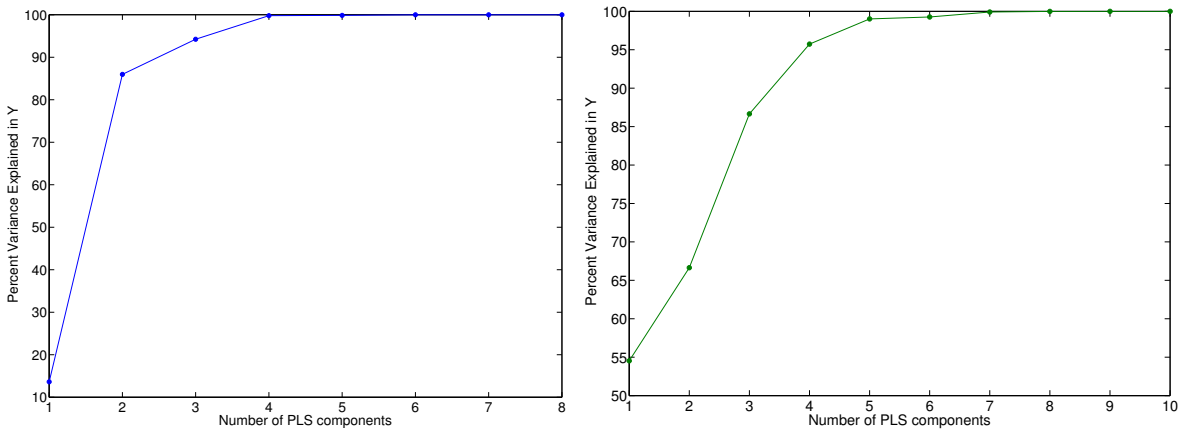

(a) Premixed Methane-air flame **(b)** Premixed Ethylene-air flame

Figure 4.8: Residual validation Y-variance versus number of PLS components used in the development of the multivariate calibration model. The left and right figures correspond to premixed CH_4 and C_2H_4 flames, respectively.

The loading-weight plot that is presented in fig: 4.9 is also essential for the development of the calibration model. The loading-weight indicates how each wavelength contributes to the determination of the equivalence ratio along each PLS-R component. For example, in fig: 4.9b, the highest the peak in the plot appears, the more the specific wavelength influences the calibration model.

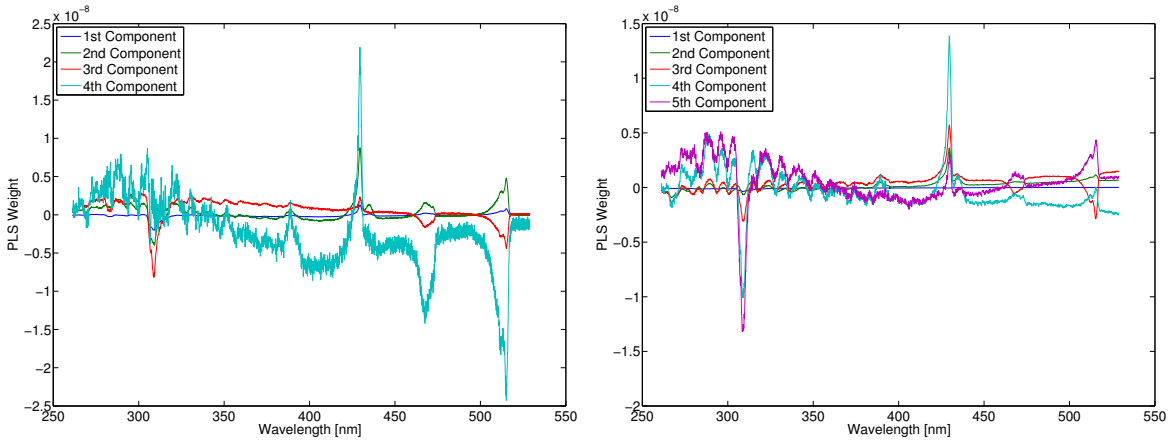

(a) Premixed Methane-air flame **(b)** Premixed Ethylene-air flame

Figure 4.9: One-vector loading weight plots along the four components of PLS for the developed multivariate calibration model. The left and right figures correspond to premixed CH_4 and C_2H_4 flames, respectively.

For the methane flame, see fig: 4.9a, in the 4th component plot, the CH and C_2 emissions seem to significantly contribute to the PLS calibration model in contrary to the OH emission that has a lot of "noise". For the contribution of OH it may be more accurate the use of 3 components, although then the contribution of the rest of the species would be quite low.

The accuracy of the PLS-R based multivariate sensing methodology is shown in fig: 4.10, where a comparison is made between the measured equivalence ratios and the ones predicted by the calibration model. The model showed adequate accuracy in both flames. The goodness of fit was $R^2 = 0.9979$ for methane and $R^2 = 0.9901$ for ethylene. The fit curve for each case separately is presented below, in fig: 4.10a and fig: 4.10b.

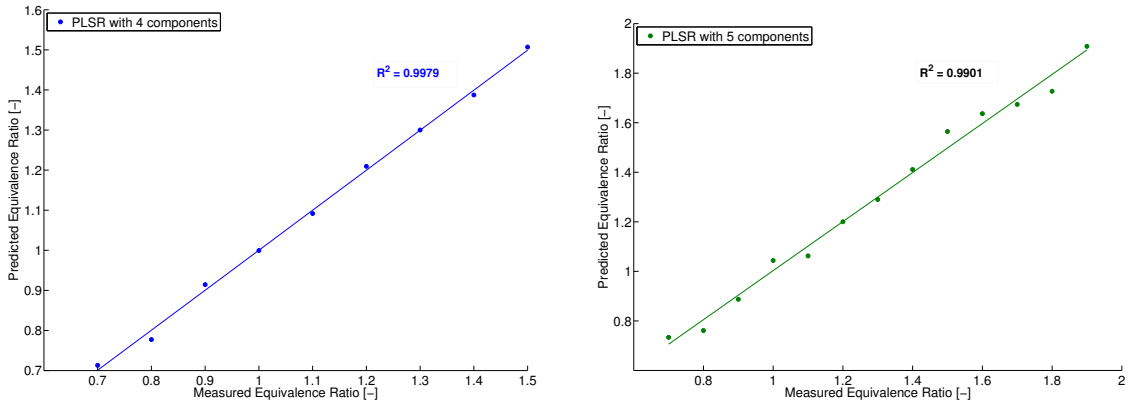

(a) Premixed Methane-air flame **(b)** Premixed Ethylene-air flame

Figure 4.10: Comparison of equivalence ratios predicted with PLS-R based multivariate calibration model and measured equivalence ratios. The left and right figures correspond to premixed CH_4 and C_2H_4 flames, respectively.

4.2 McKenna Burner with a 1.5 mm Nozzle

In this experiment, a McKenna burner with a 1.5 mm nozzle in the middle was used in order to obtain and study the chemiluminescence of a turbulent premixed ethylene-air flame, in the sooty region. The use of a burning co-flow was needed for the creation of a "shielding" environment and the protection of the jet flame from the ambient air. The burning co-flow was a premixed methane-air flame at stoichiometric conditions ($\Phi = 1.0$). In order to create a turbulent jet flame, the Reynolds number should be above 2000. The required total gas flow of the jet flame was calculated using equations (2.3), (2.4) and (2.5), the values are presented in table (4.3). The burning co-flow had a total gas flow of 40 l/min of which, 3.80 l/min were methane and 36.20 l/min were air. Measurements were taken randomly, where the presence of soot was strong in the flame and the values of the equivalence ratio were calculated afterwards.

The same experimental procedure as before was followed but in this case, only one set of measurements was taken, around 2.9 cm above the surface of the burner. Below that height, the influence from the burning co-flow was so strong that it dominated the intensity of the jet flame emission. The gain of the ICCD camera was set to 200 and the exposure time to 400 usec in order to enhance the weak chemiluminescent signal. Some of the two dimensional images that were acquired by the ICCD camera are presented in fig (4.11). The investigated area of the flame is smaller in this experiment since the diameter of the nozzle is smaller than the outer diameter of the burner. Between equivalence ratios $\Phi = 5.80 - 6.40$, additional measurements were taken, in order to determine the value, at which soot dominates over the signal. In fig (4.11c), one can notice the strong interference of soot on the right side of the picture.

Table 4.3: Gas flows in the premixed ethylene-air flame at the McKenna with a 1.5 mm nozzle burner.

Equivalence ratio (Φ)	$F_{C_2H_4}$ $[l/min]$	F_{Air} $[l/min]$
3.00	0.60	2.88
3.20	0.60	2.72
3.30	0.60	2.60
3.60	0.60	2.40
3.80	0.60	2.25
4.10	0.60	2.10
4.40	0.60	1.95
4.80	0.60	1.80
5.20	0.60	1.65
5.70	0.60	1.50
5.80	0.60	1.47
6.00	0.60	1.44
6.10	0.60	1.41
6.20	0.60	1.38
6.40	0.60	1.35
7.10	0.60	1.20
8.20	0.60	1.05
9.50	0.60	0.90
11.40	0.60	0.75

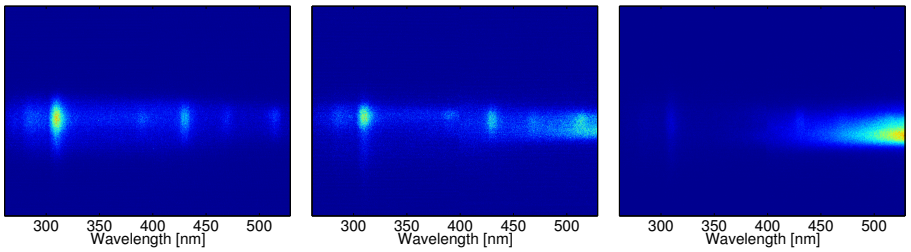

(a) $\Phi = 3.0$ **(b)** $\Phi = 5.8$ **(c)** $\Phi = 11.4$

Figure 4.11: Two dimensional images obtained by the ICCD camera, at a premixed ethylene-air jet flame of a McKenna burner with a 1.5 mm nozzle,at various Φ values. The yellow colour corresponds to a strong signal while the light blue colour represents a weaker signal.

In fig 4.12 the first head band of the OH transition ($A^2\Sigma^+ \rightarrow X^2\Pi(\Delta v = 1)$), at around 283 nm can only be observed until $\Phi = 3.3$. Above that value, only the head band at $\lambda = 308.8$ nm is apparent (Transition: $(A^2\Sigma^+ \rightarrow X^2\Pi(0-0))$). The C_2 emission is weak from $\Phi = 3.6$ until $\Phi = 5.8$ and increases again at $\Phi = 6.0 - 6.4$ until it is being dominated by the black-body radiation. The chemiluminescence of C_2 highly depends on the temperature and the equivalence ratio. At $\Phi = 3.6 - 5.8$, although the flame is rich, the temperature is not high enough to produce a sufficient amount of C_2.

We conclude that the soot domination over the chemiluminescent emission is too strong in the turbulent sooty flame. Therefore, after a certain equivalence ratio ($\Phi = 4.4$) the detection of chemiluminescence is not possible.

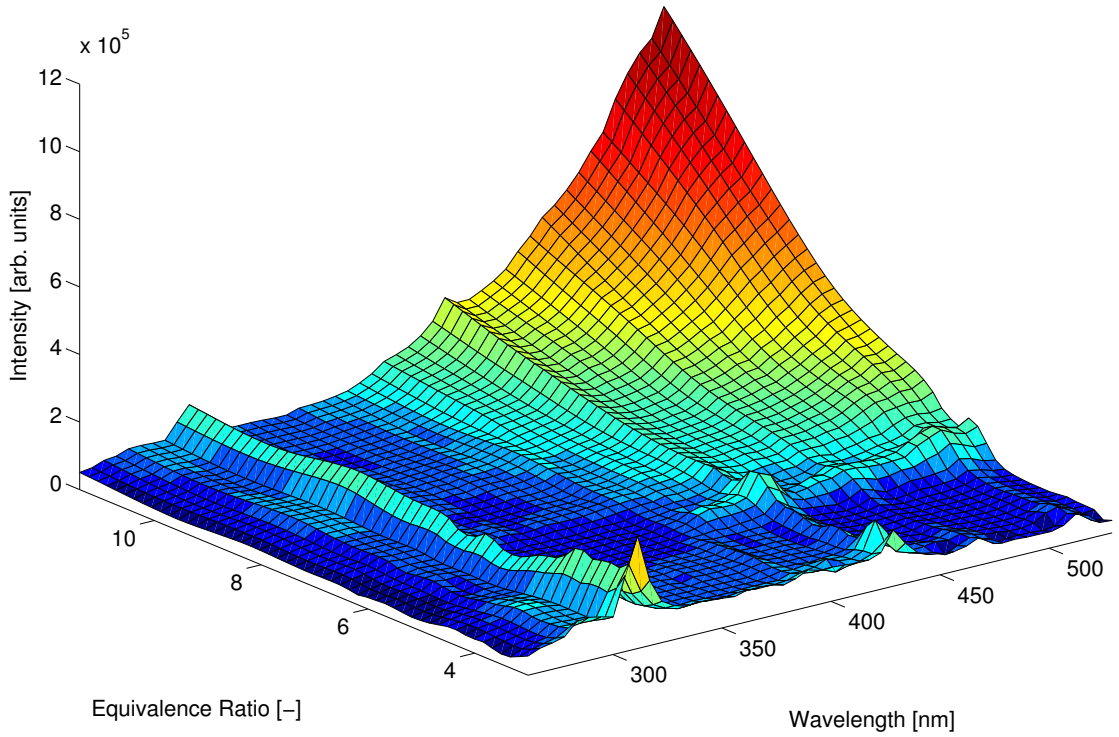

Figure 4.12: Emission spectra of a sooty premixed ethylene-air flame as a function of the equivalence ratio. The data were processed and fitted into curves in order to have a smoother visualization of the spectra. Blue and red regions correspond to weak and strong intensity, respectively.

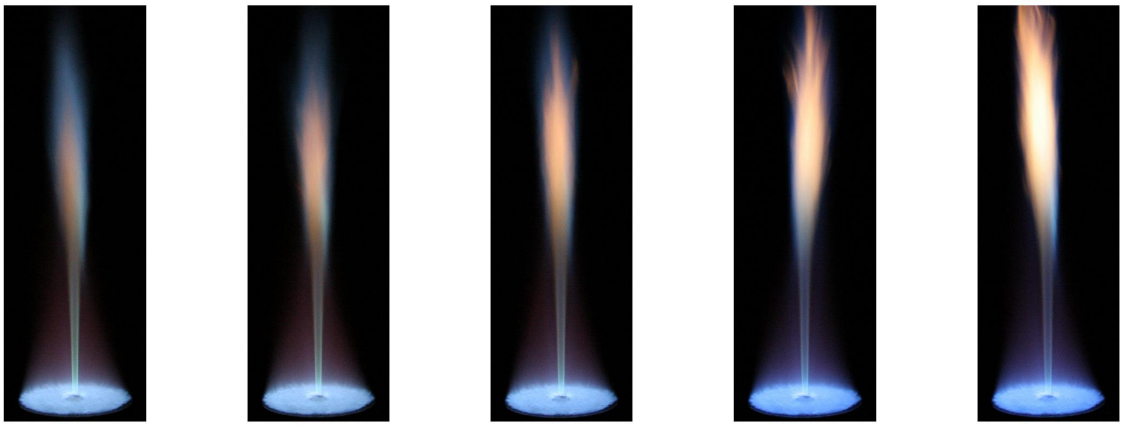

(a) $\Phi = 3.0$ **(b)** $\Phi = 3.2$ **(c)** $\Phi = 3.3$ **(d)** $\Phi = 3.6$ **(e)** $\Phi = 3.8$

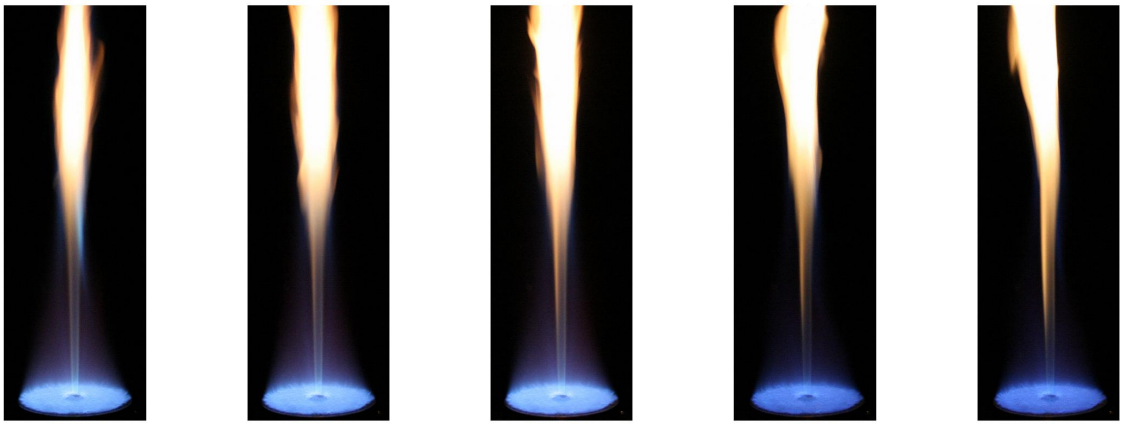

(f) $\Phi = 4.1$ **(g)** $\Phi = 4.4$ **(h)** $\Phi = 4.8$ **(i)** $\Phi = 5.2$ **(j)** $\Phi = 5.7$

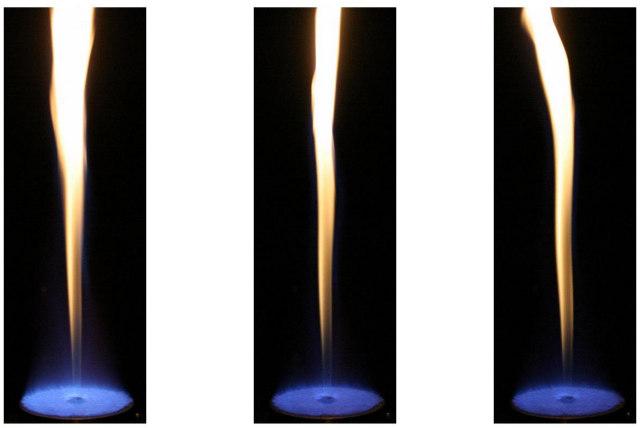

(k) $\Phi = 6.4$ **(l)** $\Phi = 7.1$ **(m)** $\Phi = 8.2$

Figure 4.13: Pictures of a premixed ethylene-air flame of a McKenna burner with a 1.5 mm nozzle), at various Φ values.

4.3 Spectral Response of Flame Sensors

Kockumation uses two different kind of flame sensors, in order to detect the presence of flame inside the burner. The UVTRON flame sensors by Hamamatsu are used in the ultraviolet region with a maximum relative rensitivity at around $\lambda = 200$ nm, see fig (4.14a). Many studies, such as *Kojima et al.* [15], *Hardalupas et al.* [11] and *Panoutsos et al. [21]* have used the OH^* chemiluminescence imaging as a technique for visualizing flames and a method for industrial sensing. Therefore, the flame sensors in the UV region should have the higher sensitivity at 260-320 nm, in order to detect the OH emission. The model that is being used in the current study, follows the curve B, which shows that above $\lambda = 300$ nm, these type of sensors cannot detect any signal. Therefore, they may detect a small part of the signal of the first headband of the OH transition, at around 282.7 nm.

The Silicon Planar Photo-transistors by Ferranti are used to detect flame in the infra-red region. The relative sensitivity of the Ferranti flame sensors reaches its maximum value at around 800 nm. These sensors have the ability to detect a part of the CH and C_2 emission. Black body radiation from soot is probably the main source that is being detected. However, the sensitivity of the sensors in the range of 400 - 500 nm, does not exceed the 30 %of the relative output.

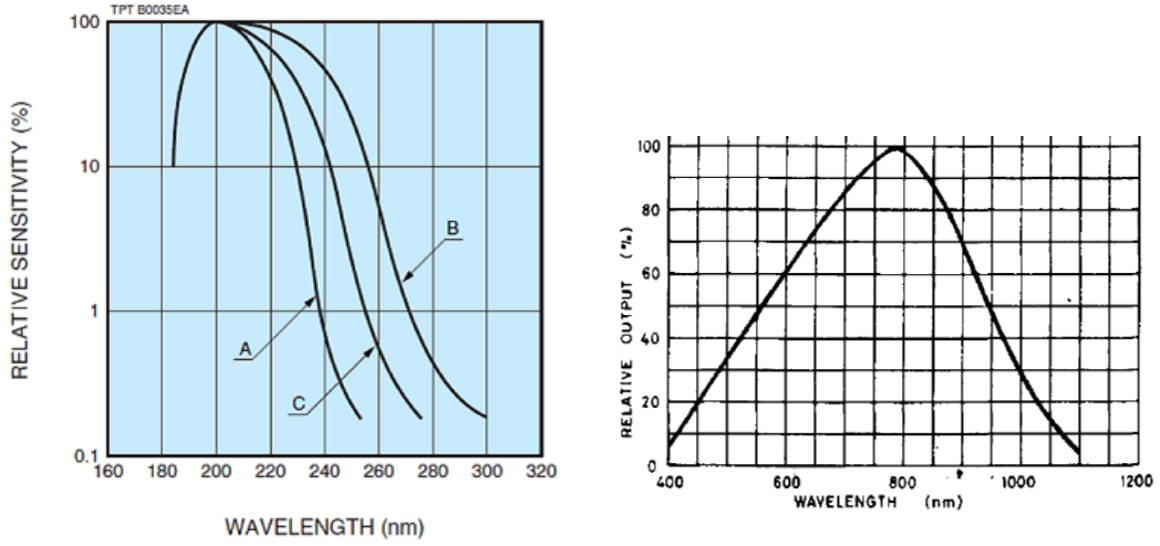

(a) Spectral response of the UV flame sensors. **(b)** Spectral response of the IR flame sensors The A,B and C curves refer to different model *(Ferranti Electronics).*
products. *(Hamamatsu).*

Figure 4.14: Relative sensitivity of the flame detectors across a certain wavelength range. In fig(a) the wavelength range corresponds to the ultra-violet region. In fig(b) the wavelength range corresponds to the infra-red region. (Figures kindly provided by *Hamamatsu* and *Ferranti Electronics*).

An alternative detection system, that could be used for flame monitoring, is the ceramic package photodiodes with low dark current by *Hamamatsu*. Photodiodes are photosensors that after the detection of light, they generate current or voltage. The spectral response (see fig: 4.15) of these detectors covers a wide range on the ultraviolet, visible and infrared wavelength region depending on the type. The Si photodiode is characterized by its high

sensitivity and low noise. Fig: 4.15 shows spectral responses for different types of Si photodiodes as well as the quantum efficiency. At a given wavelength, the number of electrons that can be extracted as a photocurrent divided by the number of incident photons is called the quantum efficiency (QS). It can be calculated using eq: 4.1.

$$QE = \frac{S \times 1240}{\lambda} \times 100 \quad [\%] \tag{4.1}$$

where S is the photo sensitivity and λ the wavelength.

The type of photodiodes which are suggested in the current study is the *S1226*. The spectral response range of the *S1226* is from 190 nm to 1000 nm, with 720 nm as a peak sensitivity wavelength. These temperature resistant detectors are suitable in detecting OH^*, CH^*, as well as C_2^* emission. One disadvantage of the photodiodes is their price, since the one unit costs approximately 10$, which is more expensive than the current detection system of Kockumation.

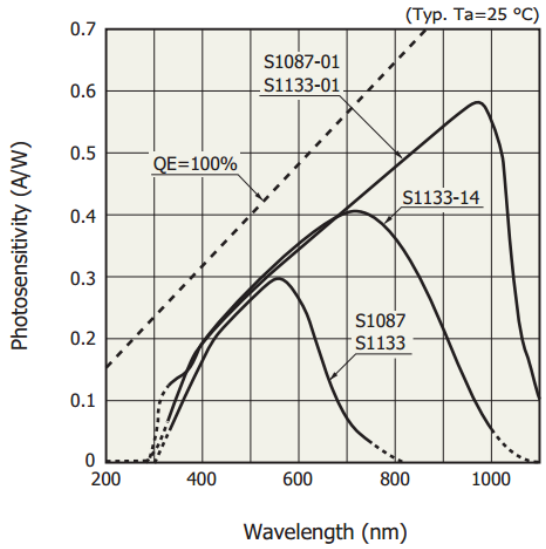

Figure 4.15: Spectral response of S1226/S1336 series UV-enhanced Si photodiodes. Each curve corresponds to a specific type of photodiodes. The dashed line shows the quantum efficiency (QE). Figure kindly provided by *Hamamatsu*.

4.4 Industrial Burner

The same experimental set-up as the one in the laboratory was used in this experiment. Measurements were taken at Pågens bakery. The industrial burner was working with danish natural gas as a fuel. The aim of this experiment was to obtain the emission spectrum of an industrial burner, more similar to the steam generator burners that Kockumation works with. In fig 4.16a, one can observe the two dimensional image, obtained by the ICCD camera. The emission of OH^* is stronger than the other radicals. Comparing the emission spectrum in fig 4.16b with the one in fig 4.2b one can notice that the spectrum of the industrial burner is similar to the spectrum of the McKenna burner, at high equivalence ratios (Φ>1) , thus in rich flames.

The emission of CO_2 contributes to the spectrum with a continuous emission that can be observed between 350 and 500 nm. NO^* and CN^* are radicals also present in flames, whose contribution to the spectrum is only significant enough in flames that highly contain nitrogen. Another factor that influences the spectrum is the background luminosity. In fig 4.16b, one can observe the two peaks of the OH^* emission at 294 nm and 318 nm. The two peaks of the CH^* emission are apparent at 395 nm and 435 nm while the two peaks of the C_2^* emission at 474 nm and 520 nm.

The peaks appear broadened and the whole spectrum seems to have been shifted around 10 nm towards longer wavelengths compared to the previous spectra from the McKenna burner. The broadened peaks is a consequence of the poor resolution of the spectrometer and its lack of success in distinguishing between rotational and vibrational bands. The shifted spectrum is probably a result of a calibration error. After the transportation of the spectrometer to the facilities Pågen, a new calibration was required, which was not made due to the lack of a suitable calibration lamp.

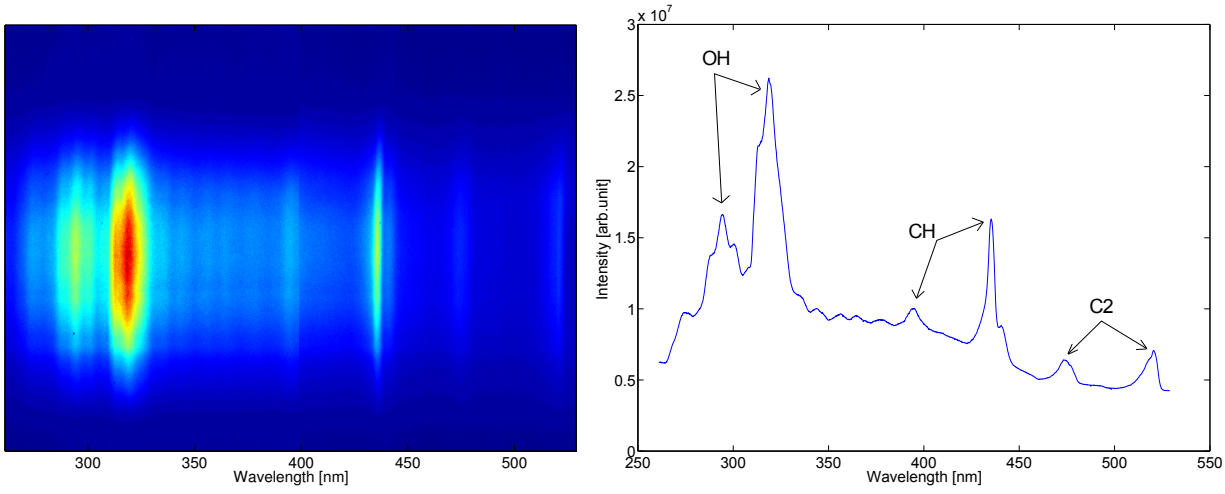

(a) Two dimensional emission image obtained by the ICCD camera. The red and the blue colour correspond to strong and weak signal, respectively.

(b) Emission spectrum of the flame.

Figure 4.16: Data from the industrial burner.

Chapter 5

Conclusions

The chemiluminescence of OH, CH and C_2 molecules has been studied at various equivalence ratios for flame monitoring, combustion control and safety checks. The aim of the current thesis is to spectrally analyse the flame emission of an industrial burner, similar to the one that Kockumation uses, a leading company in developing control systems for running boilers and steam turbines on marine vessels.

The experiments took place in the laboratory using a McKenna burner and a McKenna with a 1.5 mm nozzle burner. The studied flames were: a laminar premixed methane-air flame, a laminar premixed ethylene-air flame and a turbulent premixed ethylene-air flame. The aim of these experiments was to study the acquired spectra, to observe the emission of these molecules at different heights of the flame propagation and to use these spectra as a reference for the next set of experiments that followed.

The second part of the experimental process took place at *Pågen* bakery, a company that uses a similar burner to the one that Kockumation has in the boiler system. The industrial burner was running with natural gas as fuel. The aim of this measurement was to validate the relevance of using a McKenna burner as a substitute for an industrial burner and to compare the spectra from the two burners. The investigation of soot in the industrial burner was not successful because of the insufficient amount of soot in the flame.

After the processing of the data, the spectral response of the company's UV and IR flame sensors was compared to the acquired spectra. The sensitivity of the detectors was compared to the acquired spectra from the laboratory and from the industrial burner, in order to determine beyond which wavelength the flame sensors fail to detect a signal. A more suitable detection system is suggested in this study, the use of Si photodiodes. Although the cost might be slightly higher than the existing flame sensors, photodiodes may be more efficient in detecting the OH^*, CH^* and C_2^* emission, simultaneously. The additional use of band filters could be useful in order to detect sooty flames. By using these sensors, which are sensitive to OH*, added functionality for the system, in the form of equivalence ratio probing, could be feasible.

Furthermore, the CH^*/OH^* intensity ratio for both the methane and ethylene flame was used as a calibration method for the prediction of the equivalence ratio. This model was proved to be more accurate in the premixed methane flame than in the ethylene one. This calibration model was also compared to a new partial least square regression (PLS-R) based multivariate sensing methodology. The latter one showed adequate accuracy in the prediction of the equivalence ratio, specially in the methane flame ($R^2 = 0.9979$). These calibration models were developed for monitoring control and close-loop control of

the equivalenceratio.

The results of this study were compared to previous similar studies in order to ensure its validity. According to *Docquier and Candel* [5], in the spectra of a premixed methane-air flame the observed peaks are three for the transition of OH^*, two for the transition of CH^* and two for the transition of C_2^*. In the current thesis, the presented results are in accordance to the results by *Docquier and Candel* [5] and by *Zimmer et al.* [19]. Any difference between the spectra occurs due to the different resolution of the spectrometers that were used in each study. In fig 4.5a, at $\Phi = 1.1$, one can observe only two band heads of the OH^* transition ($A^2\Sigma^+ \rightarrow X^2\Pi(\Delta v = 1)$), at 282.7 nm and the ($A^2\Sigma^+ \rightarrow X^2\Pi(0-0)$), at 308.8 nm. The R_1 cannot be distinguished from the R_2 band head because the resolution of the spectrometer was only 300 lines/mm. The Q_2 band head is present at $\lambda = 308.8$ nm. The CH^* transition ($A^2\Delta \rightarrow X^2\Pi$) is responsible for the $Q(0-0)$ bandhead at $\lambda = 429.5$ nm and $Q(2-2)$ bandhead at $\lambda = 434.9$ nm. The swan band ($A^3\Pi_g \rightarrow X^3\Pi_u, (\Delta v = 0)$) of C_2 is responsible for the (1-1) bandhead at $\lambda = 467.6$ nm and the (0-0) bandhead at $\lambda = 515.5$ nm.

Chapter 6

Outlook

There are several research groups that have been working on chemiluminescence and its applicability on flame monitoring. The current study could be a precursor of further investigations of practical industrial burners. Some of the possible future applications are presented below.

- Further studies of spectra in the infra-red region would be very useful for the understanding of the flame behaviour and the investigation of other species involved in the combustion process.
- The NO_x emission of industrial burners plays an important role for the environmental protection. Thus, most companies are obliged to run the burners on lean conditions, in order to minimize the emission of NO_x. Additional investigation on the production and behaviour of NO_x and SO_x in lean conditions are required.
- More measurements using different type of fuels could be conducted, for example about the influence of pressure and strain to the chemiluminescent emissions. Chemiluminescence could further be used as an indicator of the flame location or heat release.
- The suggested detection system could be used in burners of large scale, such as the heating system in houses. In order to do that, further experiments should be made to test the effectiveness of the sensors.
- The calibration models that were used in the current study can be used for the prediction of equivalence ratios for unknown data sets as well as for the monitoring control of equivalence ratios in practical combustors and maybe close-loop control of the equivalence ratio.

The studies on flame spectroscopy and combustion processes could play a significant role in the future, due to the increasing demand for energy sufficiency, sustainable development and environmental awareness. The society expects the scientific community to develop a suitable algorithm that will be able to sustain the available energy, discover new resources and moreover protect the environment.

Self Reflection

A master thesis project can be quite demanding and intriguing at the same time. It is a constant battle against time, problems that may occur during the experimental process and mostly the need to exceed your own potential, proving that way to yourself and the rest that you are the right person for the job.

This project gave me the opportunity to work on a daily basis on a subject, which I have always found interesting to study, combustion physics. I have read a lot of scientific papers that provided me with a more detailed approach of experimental processes. Furthermore, the literature study helped me understand the theory and the physical aspects of my subject. Initially, a general understanding of the main field of study was needed and afterwards, the specialization in a specific area followed. Constant development of the subject by experts in the field was also taken into consideration throughout the experimental process.

Applying the theory to the actual experiment was one of the biggest challenges. There are a lot of variables that one needs to take into account for before starting the experiments, such as safety checks, getting familiar with the equipment, choosing the most suitable approach and preparing the experimental set-up. During the experimental process there are a lot of things that could actually go wrong and one must be prepared to find the most appropriate solution quickly and effectively. Dealing s uccessfully with complex phenomena without sufficient information is one of the skills that I have acquired during my thesis work.

Writing the master thesis is a procedure that can be quite tough and exhausting. Finding the right words to express yourself is not always simple. The thoughts need to be organized, the data need to be analysed and the appropriate scientific writing is required. A helpful tool in this process was the progress diary, which I was updating regularly during the whole experimental process; it was a useful reference throughout the writing.

For the first time, I was introduced to the enchanting world of research, where despite the problems that one may encounter, the satisfaction of a successful result is priceless. This project gave me the opportunity and the tools to experience the work of a scientist and I can be nothing but grateful for this.

Bibliography

[1] S.S. Ahmed, F. Mauss, G. Moreac, and T. Zeuch. A comprehensive and compact n-heptane oxidation model derived using chemical lumping. *Physical Chemistry Chemical Physics*, **9**:1107–1126, 2007.

[2] N.C. Banwell and E. McCash. *Fundamentals of molecular spectroscopy*. McGraw-Hill, 4th edition, 1994.

[3] P.E. Bengtsson. Lecture notes from the course : Fundamental combustion.

[4] Bronkhorst High-Tech B.V. *General instructions digital Mass Flow / Pressure instruments laboratory style / IN-FLOW*, 2012.

[5] N. Docquier and S. Candel. Combustion control and sensors: a review. *Progress in Energy and Combustion Science*, **28**:107–150, 2002.

[6] T. Garcia-Armingol, J. Ballester, and A. Smolarz. Chemiluminescence-based sensing of flame stoichiometry: Influence of the measurement method. *Measurement*, **46**:3084–3097, 2013.

[7] T. García-Armingol, Y. Hardalupas, A.M.K.P Taylor, and J. Ballester. Effect of local flame properties on chemiluminescence-based stoichiometry measurement. *Experimental Thermal and Fluid Science*, **53**:93–103, 2014.

[8] A.G. Gaydon. *The spectroscopy of flames*. Wiley, 1974.

[9] A.G. Gaydon and H.G. Wolfhard. *Flames: Their structure, radiation and temperature*. Chapman and Hall Ltd, 4th edition, 1979.

[10] I. Glassman. *Combustion*. Academic Press, 3rd edition, 1996.

[11] Y. Hardalupas and M. Orain. Local measurements of the time-dependent heat release rate and equivalence ratio using chemiluminescent emission from a flame. *Combustion and Flame*, **139**:188–207, 2004.

[12] Y. Hardalupas, M. Orain, C.S. Panoutsos, A.M.K.P. Taylor, J. Olofsson, H. Seyfried, M. Richter, J. Hult, M. Aldén, F. Hermann, and J. Klingmann. Chemiluminescence sensor for local equivalence ratio of reacting mixtures of fuel and air (flameseek). *Applied Thermal Engineering*, **24**:1619–1632, 2004.

[13] H.C. Hottel and W.R. Hawthorne. Diffusion in laminar flame jets. *Symposium on Combustion and Flame, and Explosion Phenomena*, **3**(1):254 – 266, 1948. Third Symposium on Combustion and Flame and Explosion Phenomena.

[14] J.A. Barnard J.F Griffiths. *Flame & Combustion.* Chapman & Hall, 3rd edition, 1996.

[15] J. Kojima, Y. Ikeda, and T. Nakajima. Basic aspects of oh(a), ch(a),and c2(d) chemiluminescence in the reaction zone of laminar methane-air premixed flames. *Combustion and Flame*, **140**:34–45, 2005.

[16] K.K. Kuo. *Principles of Combustion.* John Wiley & Sons, Inc., 2nd edition, 2005.

[17] A. Linan and F.A Williams. *Fundamental Aspects of Combustion.* Oxford University Press, 1995.

[18] A. Lipatnikov. *Fundamentals of premixed turbulent combustion.* Taylor & Francis Group, 2013.

[19] L.Zimmer, S.Tachibana, T.Yamamoto, Y.Kurosawa, and K. Suzuki, editors. *Evaluation of chemiluminescence as sensor for lean premixed combustion.* National Aerospace Laboratory of Japan, 2002.

[20] M. Orain and Y. Hardalupas. Effect of fuel type on equivalence ratio measurements using chemiluminescence in premixed flames. *Comptes Rendus Mecanique*, **338**:241–254, 2010.

[21] C.S. Panoutsos, Y. Hardalupas, and A.M.K.P. Taylor. Numerical evaluation of equivalence ratio measurement using $oh*$ and $ch*$ chemiluminescence in premixed and non-premixed methane-air flames. *Combustion and Flame*, **156**:273–291, 2009.

[22] personal contact with Bengt Månsson.

[23] M. Planck. *The theory of heat radiation.* Courier Dover Publications, 1959.

[24] S.R.Turns. *An Itroduction to Combustion - Concepts and Applications.* Mc Graw-Hill International edition, 3rd edition, 2012.

[25] M.M. Tripathi, R.S. Krishnan, K.K. Srinivasan, F. Yueh, and P.J. Singh. Chemiluminescence-based multivariate sensing of local equivalence ratios in premixed atmospheric methane-air flames. *Fuel*, **93**:684–691, 2012.

[26] European Union. Directive 67/548/eec. In Labelling The Regulation on the Classification, Packaging of Substances, and Mixtures, editors, *European Chemicals Agency*, 2009.

[27] B.B.C.G. van Elten. A cheap chemiluminescence flame sensor for central heating systems. Master thesis, Eindhoven University of Technology, 2008.

Appendix A

Abbreviations

A	Area of the flame
F	Volumetric gas flow rate
d_T	Flame quenching diameter in tube
h	Planck's constant
I	Intensity
$ICCD$	Intensified Charge-Coupled Device
k	Boltzmann constant
L	Length
MFC	Mass Flow Controller
n	Quantum number
$PLS\text{-}R$	Partial least square regression
QS	Quantum efficiency
Re	Reynolds number
S	Velocity of the gas stream
S_u	Burning velocity with respect to unburned gas
T	Temperature
U	Flow velocity
ϵ	Energy
v_b	Burning flame velocity
ν	Frequency
μ_0	Coefficient of viscosity
ν_0	Kinematic viscosity
ρ_0	characteristic density
σ	Density
σ	Stefan-Boltzmann constant
λ	Wavelength
Φ	Equivalence ratio
OH	Hydroxide
CH	Carbogen
C_2	Diatomic Carbon

Appendix B

Error estimation

The actual flow that passes through the mass flow controllers is not the same as the one that the digital box controller indicates. There are two main reasons for this variation, the uncertainty σ_f due to the mass flow controller and the uncertainty σ_{conv} due to the conversion factor. The total uncertainty depends on both σ_f and σ_{conv}. In eq: B.1 [4], the uncertainty in the flow is estimated by using the theoretical flow and the full scale of the MFC [4].

$$\sigma_f = 0.5\% \times \text{flow} + 0.1 \times \text{Full scale of the MFC} \quad [\text{l/min}] \tag{B.1}$$

The conversion factor is important when the MFC is calibrated for a different gas than the one that is actually being used. The density of the gases varies, depending on the chemical formula of the gas thus it is essential to calculate the actual flow of the used gas. This can be done by multiplying the desired flow of the used gas to the ratio: Conversion factor of the calibrated gas/Conversion factor of the used gas. If this ratio is >1 then the uncertainty is calculated by eq: B.2 [4]. On the other hand, if the ratio is <1 then eq: B.3 [4] is used.

$$\sigma_{conv_1} = 2\% \times \text{factor} \times \text{flow} \quad [\text{l/min}] \tag{B.2}$$

$$\sigma_{conv_2} = 2\% \div \text{factor} \times \text{flow} \quad [\text{l/min}] \tag{B.3}$$

The final uncertainty of the flow depends on the uncertainty due to the MFC and the uncertainty due to the conversion factor. It can be calculated by eq: B.4.

$$\sigma_{totalflow} = \sqrt{\sigma_f^2 + \sigma_{conv}^2} \quad [\text{l/min}] \tag{B.4}$$

In case of a premixed flow as the one used in the current study the uncertainty of each gas should be estimated individually, see eq: B.5 and B.6. Afterwards, the total flow is estimated using eq: B.7.

$$\sigma_{CH_4} = \sqrt{\sigma_{f_{CH_4}}^2 + \sigma_{conv_{CH_4}}^2} \quad [\text{l/min}] \tag{B.5}$$

$$\sigma_{air} = \sqrt{\sigma_{f_{air}}^2 + \sigma_{conv_{air}}^2} \quad [\text{l/min}] \tag{B.6}$$

$$\sigma_{total} = \sqrt{\sigma_{air}^2 + \sigma_{CH_4}^2} \quad [\text{l/min}] \tag{B.7}$$

For example in Table: 4.1, at Φ= 0.70, the uncertainty of the flow was estimated using the above equations at ±0.1 [l/min].

Another error that should be considered during the data process is the variation of the theoretical wavelength from the wavelength of the spectrometer. Before the experiment, the spectrometer was calibrated and the error was estimated to be ±1.2 [nm].